AALBORG UNIVERSITY

DENMARK

The isolated effect of particle surface charge on filter cake properties

Lorenzen, Søren

Publication date:
2016

Document Version
Publisher's PDF, also known as Version of record

Link to publication from Aalborg University

Citation for published version (APA):
Lorenzen, S. (2016). *The isolated effect of particle surface charge on filter cake properties*. Aalborg Universitetsforlag. Ph.d.-serien for Det Teknisk-Naturvidenskabelige Fakultet, Aalborg Universitet https://doi.org/10.5278/vbn.phd.engsci.00185

THE ISOLATED EFFECT OF PARTICLE SURFACE CHARGE ON FILTER CAKE PROPERTIES

BY
SØREN LORENZEN

DISSERTATION SUBMITTED 2016

AALBORG UNIVERSITY
DENMARK

The isolated effect of particle surface charge on filter cake properties

Ph.D. Dissertation

Den isolerede effekt af partiklers overfladeladning på filterkagers egenskaber

Ph.D.-afhandling

Søren Lorenzen

Department of Chemistry and Bioscience

Aalborg university

November 2016

Preface

This dissertation is submitted in partial fulfilment of the requirements for obtaining the degree of doctor of philosophy (Ph.D.). The dissertation consists of abstracts in English and Danish, a short thesis and four supporting papers.

Abstract

During filtration and dewatering of suspensions of biological origin, compressible filter cakes with high specific resistances are often formed. The properties of these filter cakes are significantly different from what might be expected based on classical filtration theory derived from inorganic suspensions, not only by having a higher specific resistance, but also by being highly compressible, even at low applied pressures.

One area in which this becomes an issue is in the processing of activated sludge from wastewater treatment plants, where a significant amount of operational costs are associated with either dewatering of sludge in conventional activated sludge plants, or in the prevention and/or removal of membrane fouling in membrane bioreactors. In the case of both dewatering and membrane filtration these filter cakes impose added hydraulic resistance, limiting the performance of the process.

A key factor in sludge filtration is thought to be related to the charged groups on the surfaces of the sludge flocs, single cells, and exopolymers. Literature has suggested that a reduction in these charges positively affects the filterability of sludge, mainly through increased aggregation. Some researchers have also discussed a more direct influence of charge, exerted mainly through increased osmotic pressure in the filter cake, caused by the colligative properties of the counter ions associated with the charged groups. This osmotic pressure counters the applied pressure and is therefore perceived as increased resistance, while also serving to increase the water content of the dewatered filter cake.

Due to the complexity of sludge and other suspensions of biological origin, it becomes difficult to isolate and vary only one property (such as charge) without affecting several others, all of which can affect filterability. Therefore, a set of model particles has been synthesized to allow the variation of surface charge density while keeping other properties constant. Two general types of model particles have been used in this study, both of which have a core/shell morphology and are monodisperse. The particles consists of a polystyrene core, with a highly water swollen shell made from either polyacrylic acid (PAA), hydroxypropyl cellulose (HPC), or combinations hereof. All used particles have proven to be stable against aggregation during storage regardless of particle charge, and are easily re-dispersed upon agitation.

Aqueous suspensions of the particles were used in filtration experiments to determine the filter cake properties under different operational parameters. Results

show that specific cake resistance, cake compressibility, and cake porosity increase with the particle surface charge, whereas the influence of shell to core ratio mainly affects specific resistance and compressibility, while not having a significant effect on porosity. Comparison with empirical models of filter cake resistance demonstrates that particle charge is more important than both porosity and particle size, as highly charged filter cakes have resistances orders of magnitude higher than calculated, which is not the case for filter cakes of uncharged particles.

DLVO theory suggests that the results cannot be explained in terms of classical double-layer effects, even in the extreme case of very small interparticle distances. Deviations from this classical behaviour, as suggested from literature, that arise from the confinement of charged particles by charged walls or pores are a possible explanation, allowing the high resistances to be interpreted as increased osmotic pressure due to the distribution of counter ions in the pores. Calculations indicate that osmotic pressure increases with particle charge and with decreasing porosity, but remains close to zero for uncharged particles.

Finally, filter cakes were characterized by direct optical observation of the surface of a single hollow-fibre membrane during cross-flow filtration. This method proved to be useful in terms of gaining a deeper understanding of cake growth, particle deposition, and general cake behaviour. Similar to the previously mentioned experiments, particle charge is also shown to have a great impact on both resistance and compressibility, while it was also shown to influence cake growth rate. Both compression and initial swelling of the filter cake happen within a few seconds, while further swelling could be observed during prolonged relaxation, albeit at a significantly slower rate. The degree of swelling increased with particle charge, which serves to underline the notion of an osmotic pressure in the filter cake as mentioned earlier. Lastly, the particles were shown not to attach on first contact with the filter cake, owing to the high colloidal stability due to inter-particle repulsion, yielding a cake with a high degree of order.

Dansk Resume (Danish Abstract)

Under filtrering of afvanding af suspensioner med biologisk oprindelse, vil der ofte opstå filterkager med både høj kompressibilitet og en generel høj hydraulisk modstand. Egenskaberne af disse filterkager adskiller sig markant fra den klassiske filtrerings teori afledt fra uorganiske suspensioner, ikke blot ved en højere modstand, men også ved at være meget kompressible, selv ved lavt tryk.

Et af de områder, hvor dette kan være et problem er i den videre behandling af aktivt slam fra biologisk rensning af spildevand, hvor en betydelig del af driftsomkostningerne skyldes enten afvanding af slam fra konventionelle rensningsanlæg, eller forebyggelse/fjernelse af fouling i forbindelse med membran filtrering (membran-bioreaktorer). I begge tilfælde vil den opbyggede filterkage udgøre en øget modtand, hvilket er begrænsende for processen.

En væsentlig faktor indenfor filtrering af slam, menes af være relateret til ladede grupper på overfladen af slamflokke, bakterieceller og exo-polymerer, hvor tidligere studier har fundet en positiv sammenhæng mellem bedre filtreringsegenskaber og reduktionen af disse ladninger, hovedsageligt som en konsekvens af en mere udbredt aggregering. Nogle har dog også nævnt en mere direkte indflydelse af ladningerne, gennem et højere osmotisk tryk, forårsaget af de kolligative egenskaber af ladningernes modioner. Dette osmotiske tryk vil modvirke det påsatte tryk, hvilket opleves som en højere modstand, samtidig med at det også vil øge vandindholdet af den afvandede filterkage.

Da slam og andre organiske suspensioner har meget komplekse sammensætninger, er det vanskeligt at varieret en egenskab isoleret set (som f.eks. ladning), uden at det også vil have indflydelse på flere andre egenskaber, som alle kan påvirke filtrerings processen. Dette danner baggrunden for syntetiseringen af en række modelpartikler hvilket vil give mulighed for at variere overfladeladningen samtidig med at andre egenskaber holdes konstant. To generelle typer af monodisperse modelpartikler har været anvendt i dette studie, begge med en kerne/skal morfologi. Partiklerne består af en polystyren kerne, med en kvældet skal af enten polyakrylsyre (PAA), hydroxypropyl cellulose (HPC) eller kombinationer heraf. Alle de anvendte partikler har vist sig at være stabile imod aggregering under opbevaring, uanset partikel ladning, og redisperses nemt ved agitering.

Vandige suspensioner af de producerede partikler er blevet anvendt som modelmateriale i forbindelse med filteringseksperimenter, for at bestemme filterkagernes egenskaber ved forskelligt driftsparametre. Resultater herfra viser at en øget partikelladning giver en højere hydraulisk modtand og kompressibilitet men også en større porøsitet, mens en større volumenratio mellem skallen og kernen også øger modstand og kompressibilitet, men ikke påvirker porøsiteten betydeligt.

Sammenligning med empiriske modeller for kagemodstand viser at partiklernes ladning har en større betydning end både porøsitet og partikelstørrelse, da filterkagerne fra højt ladede partikler har modstande der er flere størrelsesordner større end det beregnede, hvilket ikke er tilfældet for de uladede partikler.

Baseret på DLVO-teori, har det vist sig, at resultaterne ikke kan forklares ud fra den klassiske forståelse af dobbeltlagseffekter, selv under ekstreme betingelser med mege små afstande indbyrdes mellem partiklerne. Der er dog fundet rapporter i litteraturen der har påvist afvigelser fra den klassiske teori, hvilket opstår når ladede partikler holdes fanget mellem ladede vægge, eller i ladede porer, hvilket vil være tilfældet i en filterkage. Denne afvigelse kan være en mulig forklaring på de opnåede resulterer, da det vil forårsage en redistribuering af modioner i porevolumenet, hvilket vil øge det osmotiske tryk som opleves som en stigning i hydraulisk modstand. Beregninger indikerer, at det osmotiske tryk stiger med både partikelladning og mindsket porøsitet, mes det er tæt på nul for uladede partikler.

Afslutningsvis er filterkagerne blevet karakteriseret ved hjælp af direkte optiske observationer af fouling på overfladen en enkelt "hollow-fibre" membran. Denne metode har vist sig at være effektiv til at opnå en dybere forståelse for filterkagevækst, partikelaflejring og generelle egenskaber for filterkagen. Som i de tidligere omtalte eksperimenter, er der også her fundet en klar sammenhæng mellem partikelladning og kompressibilitet, samtidig med at partikelladningen også har vist sig at have indflydelse på vækstraten af filterkagen. Både komprimering og den umiddelbare kvældning af kagen sker indenfor få sekunder, mens længerevarende relaksation resulterer i yderligere kvældning, hvilket dog er observeret til at forgå signifikant langsommere. Kvældningsgraden øgedes også med partikelladning, hvilket understreger ideen om et øget osmotisk tryk i filterkagen, som nævnt tidligere. Slutteligt, blev det observeret, at partiklerne ikke aflejres ved den første kontakt med filterkagen, hvilket skyldes den høje stabilitet imod aggregering og leder til en filterkage med en stor grad af orden.

List of Supporting Papers

Paper I

Lorenzen S., Hinge M., Christensen M. L., Keiding K., *Filtration of Core–Shell Colloids in Studying the Dewatering Properties of Water-Swollen Materials*. Chem. Eng. Sci. 116 (2014) 558–566.

Paper II

Lorenzen s:, Christensen M. L., *Organic Model Particles with Controllable Size and Surface Charge; Synthesis, Characterization and Microfiltration Analysis*. Submitted to Powder Technol. in 2016 (under review)

Paper III

Lorenzen S., Christensen M. L., Keiding K., *The Effect of Particle Surface Charge Density on Filter Cake Properties during Dead-End Filtration.* Submitted to Chem. Eng. Sci. in 2016 (under review)

Paper IV

Lorenzen S., Ye Y., Chen V., Christensen M. L., *Direct Observation of Fouling Phenomena during Cross-Flow Filtration: Influence of Particle Surface Charge*. J. Memb. Sci. 510 (2015) 546–558.

Table of Contents

1 Introduction

Regardless of what the name suggests, filter cakes are not a new type of baked goods. They are the result of the accumulation of solid material during separation processes and are found in a variety of applications, ranging from the coffee grindings that makes the plunger on your French press hard to move to the mixture of sand, dirt, and decaying plant material that tends to clog your outdoor drain during heavy rainfall. Generally speaking, a filter cake occurs as an unavoidable consequence of the use of filters for separation purposes, as the nature of filtration is to let some components pass while leaving others behind, some of which could become the filter cake.

Dewatering and membrane micro-filtration are two related chemical unit operations widely used for separation purposes, both of which produce filter cakes. One of their many uses is in wastewater treatment, where the wastewater is treated biologically. Apart from the treated water, one main product of the treatment process is activated sludge; a complex combination of single microorganisms, sludge flocs (aggregated micro-colonies of different microorganisms), inorganic particles, bio-polymers (called EPS – extracellular polymeric substances) and un-degraded organic matter, such as fibers, as illustrated in Figure 1 [1].
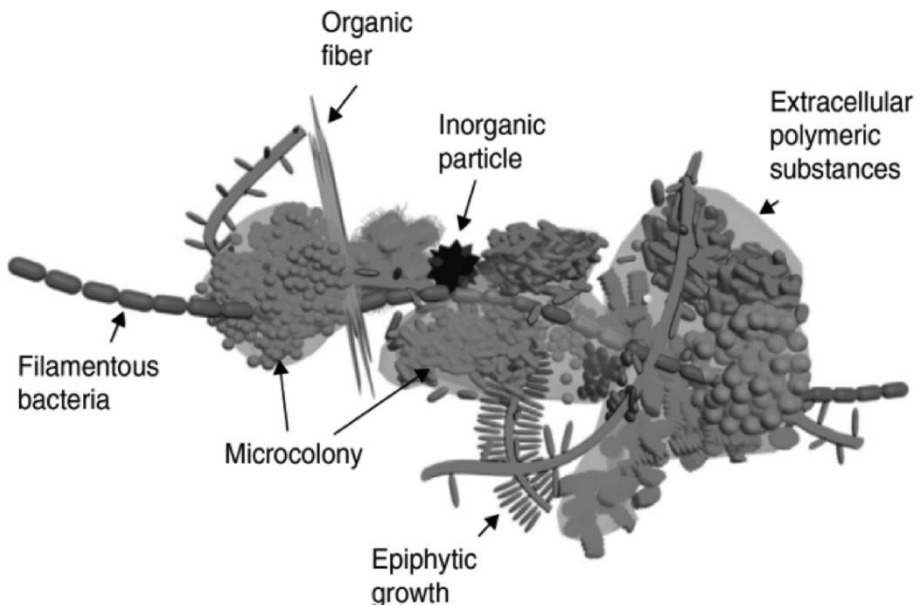

Figure 1. Illustration of the typical components of a sludge floc [1]

In conventional activated sludge plants (CAS), which have been the main treatment process the last 100 or so years [2], the activated sludge is typically removed after it has been allowed to settle in the process tanks, and have a high water content of approx. 95 - 99% [3,4]. It is desirable to remove as much water from the sludge as possible, to reduce storage and transportation needs and to reduce the energy needed for incineration. To do this, a mechanical process is typically used, often utilizing dewatering filtration alone or in combination with other processes. Here the water and the sludge particles are separated by the filter through either drainage or the application of pressure, which can reduce the water content of the filter cake to approx. 15 to 50% [3]. Dewatering processes are, however, very costly and can account for up to 32% of the total capital operating costs of the treatment plant [5]. Over the last couple of decades another wastewater treatment process has become increasingly popular [6]. This method still uses biological treatment, similar to CAS systems, but combines it with micro- or ultra-filtration, where the water is separated from the activated sludge by a porous membrane. This method, called a membrane bioreactor (MBR), has several benefits over CAS, providing a cleaner water discharge and a smaller footprint. It does however also have some drawbacks, mainly due to fouling of the membrane. Fouling occurs when components of the wastewater (both dissolved and suspended) come into contact with the membrane surface. In this sense, convection is a main contributor to fouling, as the continuous permeation of water through the membrane creates a net flow towards the membrane on the feed side, although other transport phenomena can play a role as well. Fouling changes the performance of the membrane and occurs over time, as an increasing amount of material is transported to the membrane. It can present itself in various ways, including adsorption to the membrane material, biofilm formation, gel layer formation, pore blocking, and particle deposition, i.e., the formation of a filter cake [7–11]. Both in the case of dewatering and membrane filtration the filter cake increases the hydraulic resistance, which either reduces the water flux, if the applied pressure is constant, or increases the pressure needed to maintain a certain flux. In MBRs especially, the filter cake poses a big challenge as it will continue to grow as long as the process is running, and is considered to be the dominant form of fouling, especially for long filtration times. Attempts to manage the impact of filter cakes in MBRs include cross-flow shear, relaxation, backwash, and bubbling, all of which can be effective in reducing (but not eliminating) the filter cake at the expense of higher operating costs [11–14].

It goes without saying, that the properties of the filter cake govern the process, as liquid flow through the filter cake will be a limiting factor in both of the aforementioned cases.

1.1   Cake filtration

The liquid flux through porous media (e.g., filter cakes) is often interpreted using Darcy's law, eq. 1, in which the flux, J, is expressed in terms of the pressure drop

across the cake, ΔP, the liquid viscosity, μ, and the total hydraulic resistance, R, which in turn is the sum of the intrinsic membrane resistance, R_m, and the resistance due to fouling, R_f. Typically, for organic suspensions, $R_m \ll R_f$ and can thus be neglected.

$$J = \frac{\Delta P}{\mu \cdot R} \bigg|_{R=R_m+R_f} \qquad \qquad \textbf{Eq. 1}$$

In order to properly design and dimension equipment for dewatering, knowledge is needed about the expected properties of the filter cake formed. For this purpose, semi-empirical models exist for predicting the hydraulic resistance from the cake thickness, cake porosity, liquid viscosity, and solid–liquid contact area in the cake (which can be calculated from particle size and shape). One often used model is the Kozeny–Carman model, eq. 2, giving the specific resistance, α, i.e., hydraulic resistance per cake mass deposited. Here k is the Kozeny constant (with a value of 5 $\pm$ 0.5 for spherical particles [15]), S_0 the volume specific surface of a particle, ρ_s the solid density, and ε the filter cake porosity.

$$\alpha_{KC} = k\frac{S_0^2 \cdot (1-\varepsilon)}{\rho_s \cdot \varepsilon^3} \qquad \qquad \textbf{Eq. 2}$$

Although this and some derived models are extensively used they have been shown to have several limitations. The Kozeny–Carman model has been found to give satisfactory predictions of the filtration of simple inorganic suspensions or suspensions of uncharged latex particles [16], but is very poor when dealing with suspensions of biological origin, such as microbial cell suspensions [17] or activated sludge [18] and is further complicated by the fact that it is difficult to determine S_0 and ε, especially for activated sludge. This discrepancy can also be partly due to the formation of highly compressible filter cakes, i.e., a pressure induced increase in resistance. This has previously, erroneously, been attributed to the actual physical deformation of the microbial cell or sludge floc itself, but as many species of microorganisms can maintain intra-cellular osmotic counter pressure within the range of normal filtration applications [19,20] and sludge flocs have been shown to have a compact core [21], deformation will typically not occur and the observed compression is instead due to changes in cake structure, e.g. decreased porosity.

Previous work on the filtration of wastewater sludge has found very high specific filter cake resistances, typically several hundred times higher than what would be expected from the Kozeny–Carman model, i.e., 10–100 Tm kg^{-1} [18,22–24]. Amongst the suggested explanations of this difference are blinding effects within the cake itself, which occurs when the filter cake acts as a secondary membrane,

capturing smaller particles within the pores [25,26]. But also skin (or gel layer) formation, can lead to reduced filter cake porosity, especially in layers near the membrane where the solid stress is highest, caused by the high degree of compressibility that is typical for wastewater sludge. Both of these effects are possible in systems where the suspended solids have a broad range of characteristics, which would only serve to further complicate the prediction or modelling of cake resistance. Several empirical equations exist, with the purpose of describing porosity and/or specific cake resistance as a function of pressure [27–30], the fitting parameters of which can give some information on filter cake behavior. Investigating the local porosity and solid pressure, i.e. the accumulated forces transferred to solid particles in the cake, Lu et al. (2001) used filter cakes formed from deformable particles. They found that particle deformation was responsible for the formation of a thin layer with low porosity, next to the membrane [31]. Even though sludge particles should not deform, the idea of a film/gel layer close to the membrane can still be tested using the Kozeny–Carman equation. By isolating porosity in eq. 2 one finds, using the aforementioned typical data for activated sludge, that a porosity of 0.02–0.05 is needed to explain the specific resistance of activated sludge. This is lower than the dense-layer porosity found by Lu et al. (2001), indicating that porosity is not the only factor influencing filterability [30].

1.2   Physio-chemical properties of the filter cake

As sludge is a very complex matrix [32], it is difficult to isolate and vary only one property of a sludge floc, in order to investigate the influence of different physio-chemical properties, without affecting several others, all of which can affect filterability. In this context, Hodgson et al. found that manipulating the surface properties of bacterial cells significantly affected filtration behaviour, with filter cake resistance decreasing as the matrix of extracellular polymeric substances (EPS) outside the cell wall was removed [19]. Both the physical appearance of the cell and the influence of EPS removal on specific resistance are shown in Figure 2.
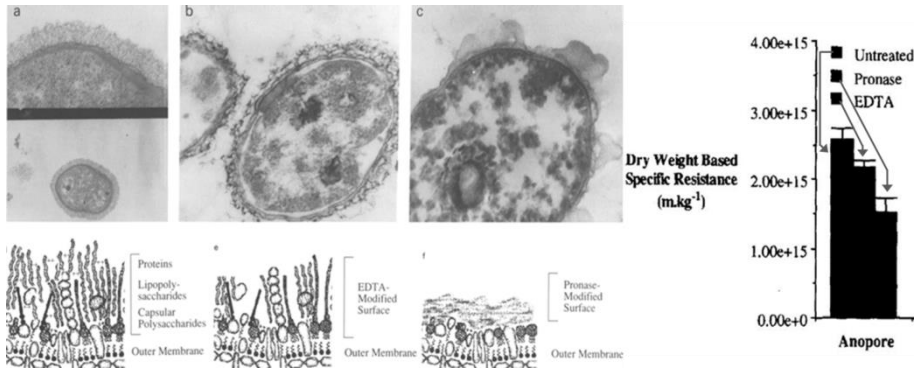
Figure 2. Surface modification of bacterial cells and the impact on filter cake resistance [19].

Later Ohmori and co-workers found that both pH and ionic strength affected filtration resistance, Figure 3 right, which was correlated with charged groups on the EPS surrounding the cells [33], while adsorption of amino acids to the cell surface, Figure 3 left, had a similar effect [34]. In addition, growth medium was found to affect filtration as the properties of the bacterial cell wall changed in response to growth conditions [35]. This infers that particle surface properties, especially charge density, is an important factor in the filtration of organic matter.
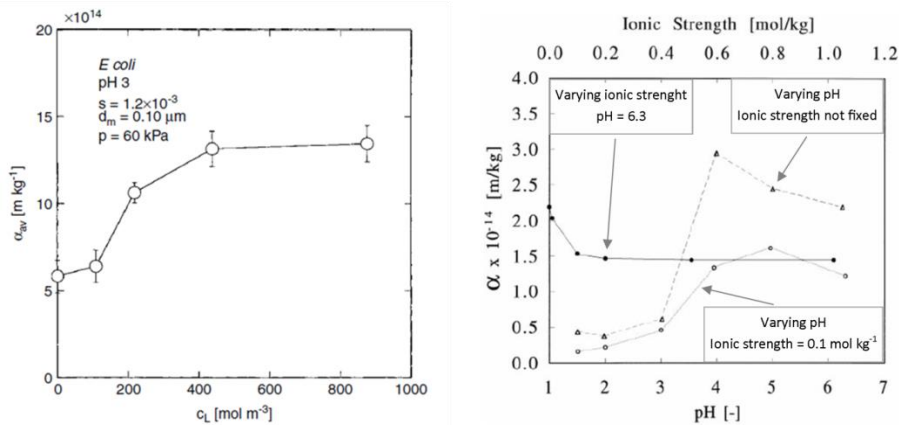
Figure 3. The effect of amino acid (left) adsorption and variations in pH and ionic strength (right) on filter cake resistance [33,34]

Indeed, one of the key factors in sludge filtration is thought to be related to the charged groups on the sludge flocs, single cells, and exopolymers. In line with the mentioned findings of Hodgson, Ohmori, Glatz and Iritani, it has been found that variations in charge density affects the filterability of sludge [18,36]. This is

presented in Figure 4 a, where the relative amount of EPS to calcium and iron ions is shown to influence floc strength (expressed as mean floc size over turbidity), while Figure 4 b shows how floc strength affects filter cake resistance. As both calcium and iron ions bind to negative charges on the EPS, effectively neutralizing it, a low ratio of EPS to these ions will result in strong flocs, Figure 5 left, while a high ratio increases the repulsion between the components of the floc, making it deflocculate into smaller particles and free EPS, Figure 5 right.
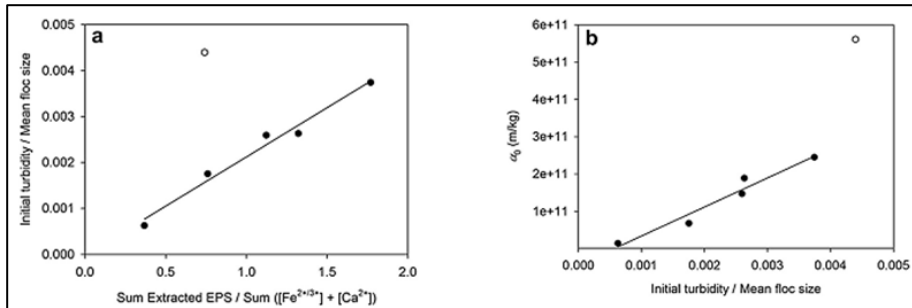
Figure 4. Effect of EPS on filter cake specific resistance through changes in the relation between flocs and smaller particles, i.e., floc strength [36]

As both calcium and iron ions bind to negative charges on the EPS, effectively neutralizing it, a low ratio of EPS to these ions will result in strong flocs, Figure 5 left, while a high ratio increases the repulsion between the components of the floc, making it deflocculate into smaller particles and free EPS, Figure 5 right.

| Very good compact flocs | Good flocs | Deflocculated/ poor flocs |
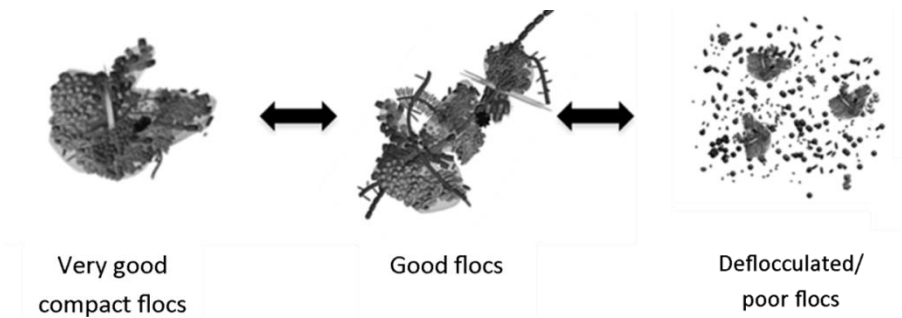
Figure 5. Illustration of a sludge floc as charge density goes from low (left) to high (right), leading to deflocculation [1]

Some researchers have also discussed a more direct influence of charge exerted mainly through increased osmotic pressure in the filter cake, caused by the colligative properties of the counter ions associated with the charged groups. This osmotic pressure counters the applied pressure and is therefore perceived as an

increased resistance [37,38]. This effect has only recently been quantified in MBR systems [39–42], while earlier work has found osmotic pressure to be negligible in cross-flow microfiltration [43]. The complexity and diversity of sludge, however, will make it difficult to compare results and might even lead to contradictory conclusions, as the effect of charge is impossible to isolate due to the adverse secondary effects occurring when attempting to vary the charge density, such as changes in floc strength and particle size distribution.

Instead model particles could be a useful tool to simulate real-world suspensions, while also having the added benefit of ruling out effects caused by blinding and skin formation, given the right particle properties.

1.3   Synthetic particles as model material

To overcome the inherent complexity of sludge and other suspensions of biological origin, synthetic model particles have been extensively used for filtration purposes for a number of years [30,44–52]. Model particles can provide a simplified system with well-known parameters, allowing for more in-depth investigations of the influence of these properties on the filtration process, while still maintaining some similarity with the complex system in question. An example of this could be the use of core/shell particles to mimic the single bacterial cells mentioned previously, as the particle core represents the cell itself while the shell represents the EPS layer attached to the outside of the cell wall.

Depending on the context and problem to be investigated, numerous classes of model particles exist. Silica and other types of inorganic particles are found mainly as nanoparticles, 10–500 nm in size [53,54]. They offer the benefits of being spherical and rigid, with high chemical resistance, while monodispersity is typically easy to achieve. Furthermore, they have a negatively charged surface that responds to changes in pH [54]. They do, however, have a high density, so sedimentation can be an issue. Organic polymer particles, on the other hand, offer much more flexibility [55,56]. Depending on the manufacturing method they can range in size from a few nanometres to several micrometres, and some methods produce highly monodisperse suspensions [57]. Organic polymer particles also exhibit flexibility with regard to choice of material and, depending on the polymers used, many particle properties and combinations thereof can be obtained [57,58]. The most common way to produce organic polymer particles is by a heterogeneous polymerization process [59].

One such process is emulsion polymerization, a method that is very versatile and easily forms monodisperse particles in bulk quantity, however, particle sizes are typically in the nanometre scale [30,59]. Although emulsion polymerization can give rise to a wide array of particle properties, it is difficult to vary only one property without affecting others as well. For example, attempts to increase the surface

charge density will result in smaller particles due to increased stabilization, while increasing the charge density of core/shell-type particles will increase the volume ratio between the shell and the core.

Another often used method is dispersion polymerization [57,60,61], which yields monodisperse particles with a core/shell configuration. On the other hand, dispersion polymerization typically produces particles in the 1–10-µm range, although sub-micron sizes as well as sizes up to 15 µm have also been reported [62]. This method has another advantage as well, offering better control over shell thickness due to a different stabilizing mechanism during the synthesis. The method, however, does not offer much control over surface charge density, as this value needs to fall within a certain limit for monodispersity to occur.

A third option would be simply to buy the particles needed, for example, from a chemical supplier, as they often offer monodisperse particle standards. However, this is very costly, especially considering the volume of particles needed to conduct filtration experiments.

Despite the great variety of available model particles and single microbial cells, none of the commonly available particles/cells can be used to investigate the isolated influence of surface charge. As long as surface charge is the only, or at least the dominant, source of stability towards aggregation secondary effects will always be present, i.e., aggregation, changes in shell volume, collapse of polymers, swelling/deswelling of the particle, and so on. Obtaining a filtration setup in which particle surface charge is the only variable requires model particles with a particular set of properties. The particles will have to be: monodisperse (no blinding effects), spherical (to allow for simple geometric calculations), similar in size to microbial cells (0.5–5 µm in size), chemically stable (properties should not vary over time and no detachment of charged groups should occur), rigid (to rule out particle deformation), close to the density of water (to reduce the effect of sedimentation), and finally, stable towards aggregation regardless of the surface charge density [59].

In this project, core/shell particles fulfilling all of these requirements, while having a shell thickness comparable to the EPS layer, were produced by emulsifier-free emulsion polymerization and a modified dispersion polymerization technique specifically developed as a part of the project.

1.3.1 Emulsifier-free emulsion polymerization

In classical emulsion polymerization, a schematic overview of which is shown in Figure 6, the main monomer is only slightly soluble in the polymerization medium, as in the case of styrene in water (solubility is approx. 4 g L^{-1}). Instead, the monomer is kept in suspension by the use of emulsifiers, e.g., soap, which stabilizes both the larger monomer droplets, while also forming empty micelles and monomer-filled

micelles, typically between 5-10 nm in size. Initiation of polymerization is carried out by the use of a water soluble initiator (typically persulfate salts), and the locus of initiation will therefore be in the water phase, hence the need for a slightly soluble monomer. Once initiated, oligoradicals are produced and adsorbed by the monomer micelles, allowing the further polymerization within the micelle as more monomer continuously diffuses from the larger droplets into the micelles. Eventually the monomer will be completely consumed and polymerization will stop, leaving behind emulsifier stabilized particles [57].

Emulsifier-free emulsion polymerization will, as the name suggests, not utilize emulsifiers for micelle formation and particle stabilization. Instead, this method relies on *in-sit*u production of stabilizing polymers, and are thus often performed as a co-polymerization between the slightly soluble monomer mentioned before and a highly soluble monomer, whose corresponding polymer is also water soluble. This co-polymerization will eventually form micelles and stabilize the growing particles as before, creating a core/shell type particle. By varying the ratio between the two monomers, the shell to core volume ratio can be controlled, which is utilized in this project [57,63].
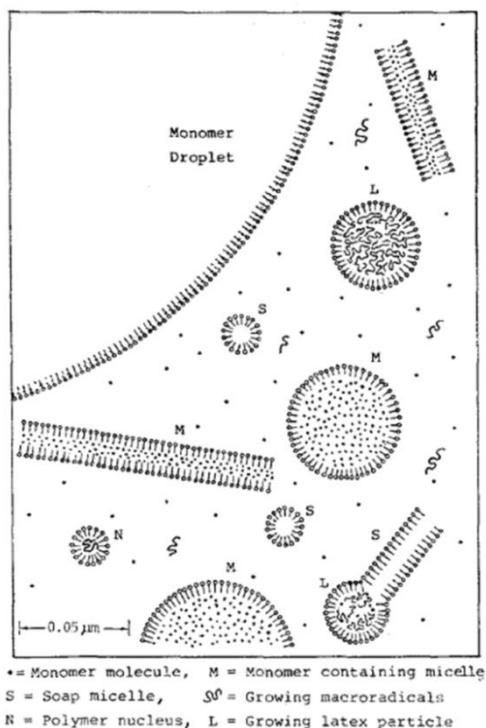
Figure 6. Schematic overview of the particle formation during emulsion polymerization [57]

1.3.2 Dispersion polymerization

In dispersion polymerization, a schematic overview of which is shown in Figure 7, all starting components are dissolved before initiation, typically in short-chain alcohols. Polymerization is initiated in the homogeneous mixture and oligomers will start to form due to solution polymerization. As the chains grow, they will eventually precipitate and form small nuclei due to the insolubility of the growing polymer. These nuclei will then grow into particles, as they act as scavengers, coalescing with other nuclei, capturing the still-growing oligomers, and also becoming swollen by monomers diffusing from the solution into the nuclei. This allows the captured oligomers, still containing a free radical end group, to undergo bulk polymerization within the particle, much as in emulsion polymerization. Simultaneously, the stabilizer will anchor to the particle preventing the coalescence of larger particles, while still allowing the scavenging of small nuclei and oligomers that are not yet stabilized.
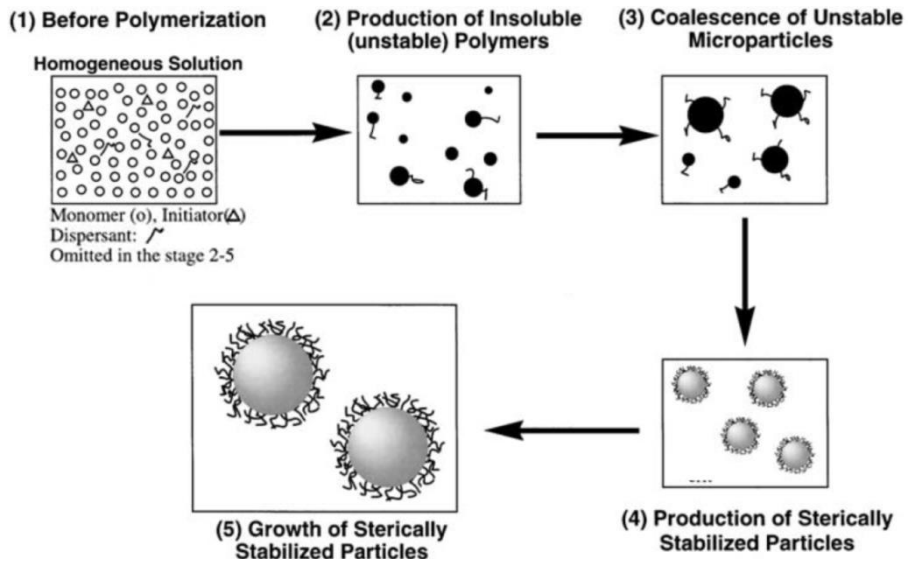
Figure 7. Schematic overview of the particle formation during dispersion polymerization [60]

Solution polymerization occurs throughout the synthesis, as such new oligomeric radicals and even new unstable nuclei can form, possibly leading to the production of secondary particles. However, under favourable conditions, these products of solution polymerization will be scavenged by existing larger particles before they can grow into mature particles [64]. The final size and size distribution of the produced particles depend on several factors, such as reaction temperature, initiator concentration, monomer concentration, solvent composition, stabilizer molecular

weight (MW), stabilizer concentration, and polymerization kinetics, including chain transfer and polymer propagation rates. The interplay between these factors has previously been investigated by others [60,64–66]. Stabilization is crucial in the particle formation stage and is introduced by chain transfer to the polymeric stabilizer, as illustrated in Figure 8.
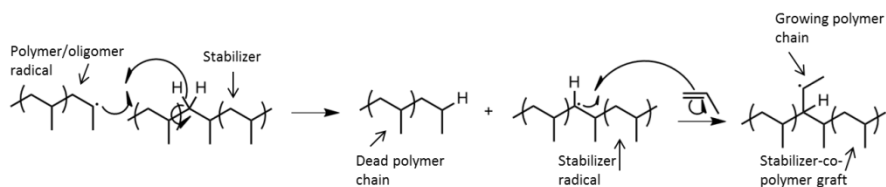
Figure 8. Reaction pathway of the chain transfer mechanism

This produces an H-terminated compound (where the free radical was before) and a new free radical on the α-carbon. Due to the electron-donating properties of the functional groups on the polymeric stabilizer, this new free radical is stable enough to propagate with monomers in solution, creating a chain of poorly soluble polymer, i.e., the anchor, grafted to the highly soluble stabilizer[67]. The anchor part is incorporated into the particle with a still-active free radical chain end, which will further propagate inside the monomer-swollen particle. This will make the anchor covalently linked to the particle This makes removal of the stabilizer from the particle highly unlikely [68]. The anchored stabilizers will form a "hairy" layer surrounding the particle [64], the thickness of which depends on the MW of the stabilizer, as well as polymer-polymer and polymer-solvent interactions.

In this way, stabilization is generally achieved by either steric or electrostatic repulsion, depending on the properties of the stabilizing polymers and the solvent. It is through the combination of these two effects that control over particle surface charge becomes possible, by increasing the amount of steric stabilizer when the electrostatic stabilizer decreases – a novel approach for controlling surface charge without introducing secondary effects.

2 Objectives

The objective of this PhD project is to gain knowledge about the influence of particle surface charge on filter cake behaviour during filtration of well-defined organic model particles, specifically made to simulate the particles found in activated sludge and other suspensions with similar properties. The main focus will be on specific filter cake resistance, compressibility, porosity, and osmotic effects.

It is well known, that the properties of suspended solids in activated sludge have an effect on filtration performance, but the high complexity and variety of sludge makes investigation of the isolated effect of these properties difficult. Even though model particles have previously been used extensively for similar purposes, the ability to vary particle charge without varying other properties has not existed until now.

This project will concern:

1) The development and production of novel synthetic model particles from organic polymers. The aim is that these particles should be able to mimic some of the properties of wastewater sludge, while still having the opportunity to vary surface charge density without compromising other properties.

2) Dead-end filtration experiments to determine how particle surface charge influences filtration and dewatering behaviour. This can contribute to a better understanding of the impact of particle fouling when designing and running MBRs and can serve to improve dewatering of waste activated sludge.

3) The use of real-time direct observation as a method to provide a deeper understanding of the formation and behaviour of filter cakes, including particle deposition, compression/swelling and cake removal.

3   Synthesis and characterization of model particles

Due to the high complexity of suspensions of biological origin, model particles were chosen as a tool to investigate the influence of particle charge on filterability, filter cake properties, and particle deposition. Model particles can provide a simplified system with well-known parameters, allowing for more in-depth investigations of the influence of these properties on the filtration process, while still maintaining some similarity with the complex system in question. An example of this could be the use of core/shell particles to mimic the bacterial cells mentioned previously, as the particle core represents the cell itself while the shell represents the EPS layer attached to the outside of the cell wall. For the bacteria used by Hodgson et al. [19], the EPS layer accounts for approx. 10-20 % of the total cell diameter.

The general requirements for model particles useful for the presented study are:

- Well characterized, in terms of particle size, size distribution, composition and charge density;

- Monodisperse, to avoid blinding effects;

- Spherical, to allow for simple geometric calculations;

- Within the same order of magnitude as microbial cells;

- Control over specific physio-chemical properties;

- Chemically stable, i.e., properties should not vary over time;

- Close to the density of water, to reduce the effect of sedimentation;

- Stable towards aggregation.

Two general types of model particles have been used in this study, both of which have a core/shell morphology. The particles consisted of a polystyrene core, with a highly water swollen shell made from either polyacrylic acid (PAA), hydroxypropyl cellulose (HPC) or combinations hereof. The core material was chosen as it is hard and incompressible (at the pressure ranges used during filtration), resembling the nature of bacterial cells [69] and the interior of sludge flocs [18], while the shell would make a gel-like soft surface, similar to the EPS present on the surface of the cells and the sludge flocs. The particles differ in two distinct ways. In terms of size,

with particle type I being smaller than 500 nm and particle type II being larger than 1.4 μm; and in terms of shell composition, with particle type I having a shell made from PAA but varying in thickness, while particle type II has a shell with a fixed thickness, but composed of mixtures of PAA and HPC.

3.1 Type I – small core/shell particles with variable shell thickness

Made from emulsifier-free emulsion co-polymerization of styrene and PAA, the particles fulfilled all of the aforementioned requirements, with the added benefit of being able to control particle charge by varying the shell to core ratio. This allowed the influence of not only charge density, but also shell thickness to be investigated.

The amount of acrylic acid incorporated in the purified particle suspensions was determined by potentiometric titration of acidified samples using 25 mM sodium hydroxide as titrant. Results showed a linear relationship between the amount of acrylic acid added to the synthesis and the concentration of carboxylic groups (per gram dry matter), *CA*, as shown in Figure 9. The titration method used was developed for titrating polymer solutions, so it is unlikely that carboxyl groups encapsulated in the PS matrix will be detected by the performed titrations. As such, the carboxylic groups found by titration are assumed to be from the surface of the particles [30]. Particle size and size distribution was determined by dynamic light scattering and showed the particles to be monodisperse within each batch. The measurements were made at pH 3 (Dc) and pH 9 (Ds), and in all instances the hydrodynamic radius was found to be largest at pH 9. This was expected due to dissociation of the carboxylic group and the resulting swelling of the PAA shell [30].

Combined, the titration results (charged particle surface) and the dynamic light scattering measurements (particles swell at high pH) indicates that the produced particles have a core–shell morphology, in good agreement with the literature, where the surfactant-free emulsion copolymerization process is known to yield mono-disperse core–shell composite particles [30,70].

The ratio between the volume of the fully swollen shell and the total particle volume, denoted ψ, was calculated from eq. 3, with D_s being the swollen diameter (high pH) and D_c the diameter with a collapsed shell (low pH). Shell thickness ranged from 21 to 124 nm, and increased linear with the amount of acrylic acid added during the synthesis, as shown in Figure 9 [30].

$$\psi = \frac{D_S^3 - D_C^3}{D_S^3}$$

Eq. 3
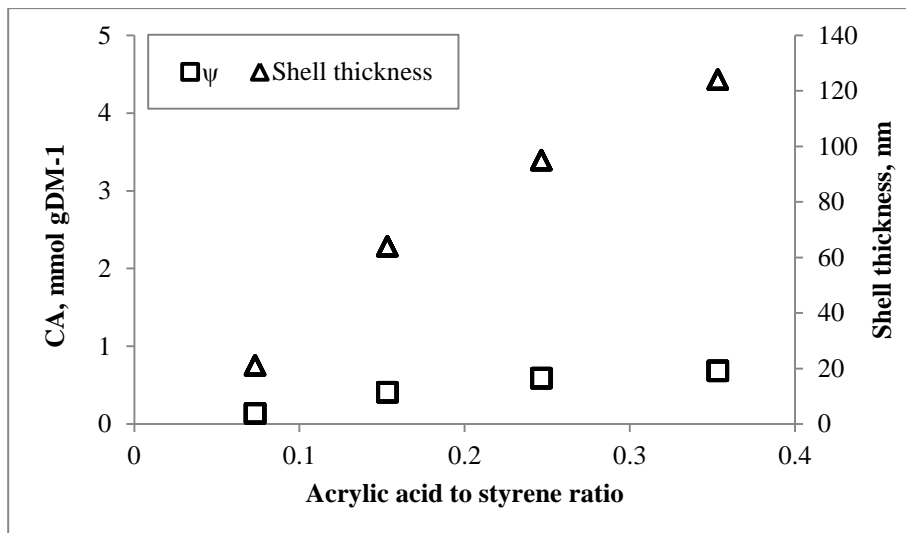
Figure 9. Charge concentration and shell thickness as a function of the ration between acrylic acid and styrene added during synthesis [30]

Table 1. Summary of the measured physicochemical properties of the PSA particles. D_c = hydrodynamic diameter at low pH (collapsed shell), D_s = hydrodynamic diameter at high pH (swollen shell), ψ = volume fraction of water-swollen shell relative to entire particle. The values in boldface are estimated values [30]

ID (–)	D_c (nm)	D_s (nm)	ψ
PSA90/0	431	452	0.133
PSA82/0	337	401	0.406
PSA74/0	276	371	0.588
PSA67/0	268	392	0.680
PSA86/0	267	276	0.095
PSA86/0.5	350	362	0.096
PSA86/1.0	431	448	0.11
PSA86/1.5	447	463	**0.1**
PSA86/1.75	461	478	**0.1**
PSA86/2.0	480	497	**0.1**

Even though this type of particle has the benefit of simulating EPS covered microbial cells, combining the effects of surface charge with a water-swollen gel-like material, they do, however, also have some drawbacks. At around 400 nm, the particles are smaller than the typical components found in biological suspension, and as the shell to core ratio increases, particle size decreases even further. This could lead to an overestimation of surface related effects, as these tend to increase when particle size decreases (volume specific surface area is inversely proportional with particle radius). Furthermore, the direct influence of charge is difficult to isolate, as a change in surface charge is always accompanied with changes of other particle characteristics, i.e., particle size, shell to core ratio and stability towards aggregation (if surface charge gets to low). Besides varying the shell to core ratio, the same particle type was made with different diameters, all with the same shell to core ratio. Detailed information regarding synthesis and characterization are presented in supporting paper I [30], with a summary of particle characteristics shown in Table 1.

3.2 Type II – larger core/shell particles with variable surface charge density

Based on the aforementioned limitations, a second type of model particle were produced [59]. These particles were made by modifying the dispersion polymerization of styrene in methanol, with soluble pre-made polymers as stabilizers. During the polymerization, stable particles are achieved by a chain-transfer mechanism, where free radicals are transferred to the stabilizing polymers. These activated polymers can then react with styrene monomers in solution to create a T-shaped graft-polymer, where one end is highly soluble in the solvent, whereas the other end (the polystyrene part) is not. The polystyrene part is incorporated into the particle with a still-active free radical chain end, which will further propagate inside the monomer-swollen particle. This will make the anchor covalently linked to the particle, as illustrated in Figure 10 [68].
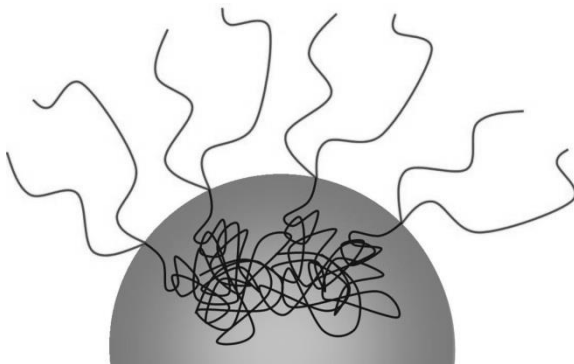
Figure 10. Schematic (not to scale) of a particle (grey) with a graft co-polymer whose anchor part (black) is buried inside the particle and soluble part protrudes from the surface [59]

The anchored stabilizers will form a "hairy" layer surrounding the particle [64], the thickness of which depends on the molar weight of the stabilizer.

Generally speaking, stabilization is achieved by either steric or electrostatic repulsion, depending on the properties of the stabilizing polymers and the solvent. It is through the combination of these two effects that control over particle surface charge becomes possible, by increasing the amount of steric stabilizer when the electrostatic stabilizer decreases – a novel approach for controlling surface charge without introducing secondary effects. In this study, two different stabilizing polymers were used, being the charged polymer, polyacrylic acid (PAA), and the uncharged polymer, hydroxypropyl cellulose (HPC), both of which have a high solubility in both methanol and water.

These particles were made bigger than type I, but maintained the core/shell structure, while also fulfilling all the listed requirements. For this type, the ratio between the volume of the fully swollen shell and the total particle volume were approx. 0.2. These particles proved stable towards aggregation, regardless of surface charge, due to the combination of steric and electrostatic stabilization [59].

The size distribution of the particles can be given as the grade of polydispersity, δ, calculated from eq. 4, where d_i is the particle diameter below which i % of the particles are found. If $\delta < 0.14$, the particles are defined as being truly monodisperse, whereas if $0.14 \leq \delta \geq 0.41$, the particles are considered quasi-monodisperse [71].

$$\delta = \frac{d_{84} - d_{16}}{2d_{50}} \qquad\qquad \textit{Eq. 4}$$

Particle characterization showed the particle size to be constant, regardless of shell composition, with the exception of particle E, while all particles have a narrow size distribution, indicated by the low grade of polydispersity. Table 2 provides an overview of particle size and size distribution, δ.

The values given in table 2 were confirmed by SEM images of the particles, as shown below in Figure 11, which also confirms a spherical shape. Due to the incomplete collapse of HPC onto the particle surface during drying (in preparation for SEM), some particles also show visible shell polymers on the particle surface, confirming that the method indeed results in a core/shell morphology and that the polymeric stabilizers are evenly distributed across the particle surface (Figure 11, bottom right).

Table 2. mean size (μm) and grade of polydispersity of the produced particles measured using laser diffraction [59]

Particle ID	Mean size (μm)	Grade of polydispersity, δ
A	1.36	0.17
B	1.41	0.15
C	1.37	0.15
D	1.41	0.14
E	2.21	0.15
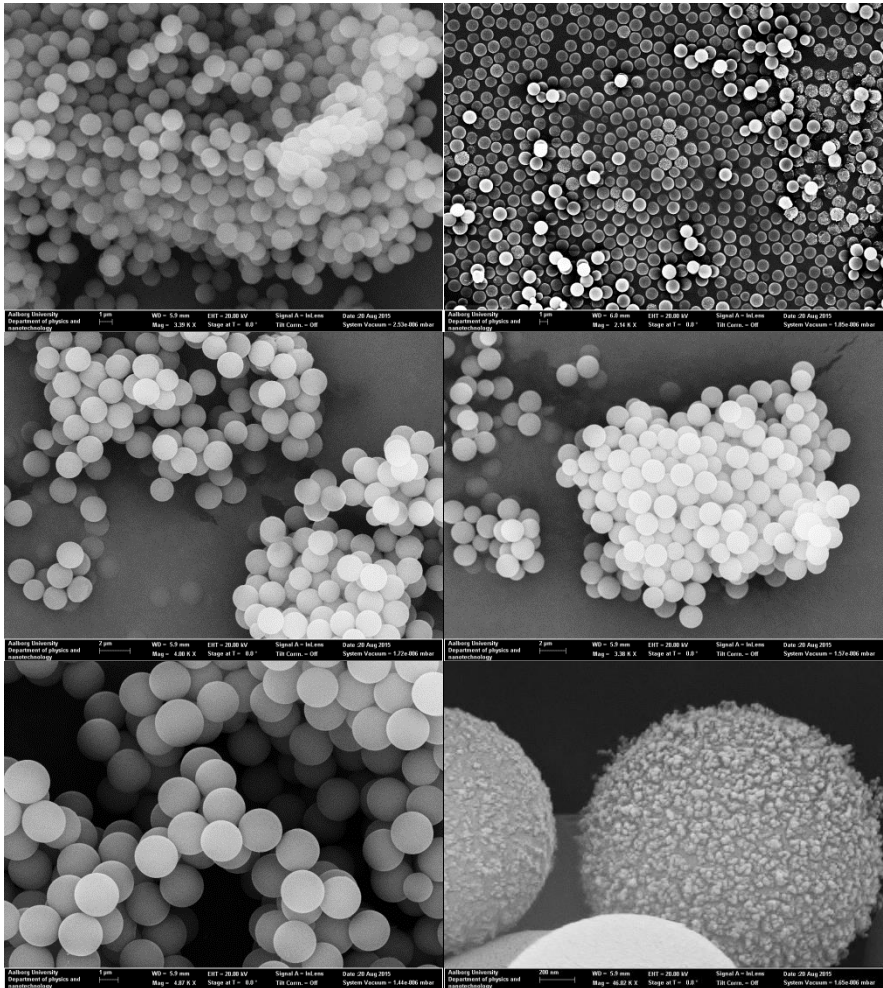
Figure 11. SEM images of the produced type II particles. A, top left; B, top middle; C, top right; D, bottom left; E, bottom middle. Bottom right picture shows a high magnification of particle C, with visible shell polymers on the surface [59]

The weight ratios in % of PAA to HPC used in the synthesis were 0:100, 25:75, 50:50, 75:25, and 100:0, yielding particles ranging from uncharged to highly charged. The measured electrophoretic mobility of the particles is shown in Figure 12, with the mobility increasing linearly with PAA wt.%. Although the concept of zeta-potential loses its meaning for core/shell particles (the surface of shear is not well defined), electrophoretic mobility is still inherently connected to the charge density of the particle shell through the equations of Ohshima [59,72].

Further surface analysis showed good agreement with theory in terms of grafting density (distance between polymers on particle surface) and shell thickness, which is discussed in greater detail in supporting paper II [59].
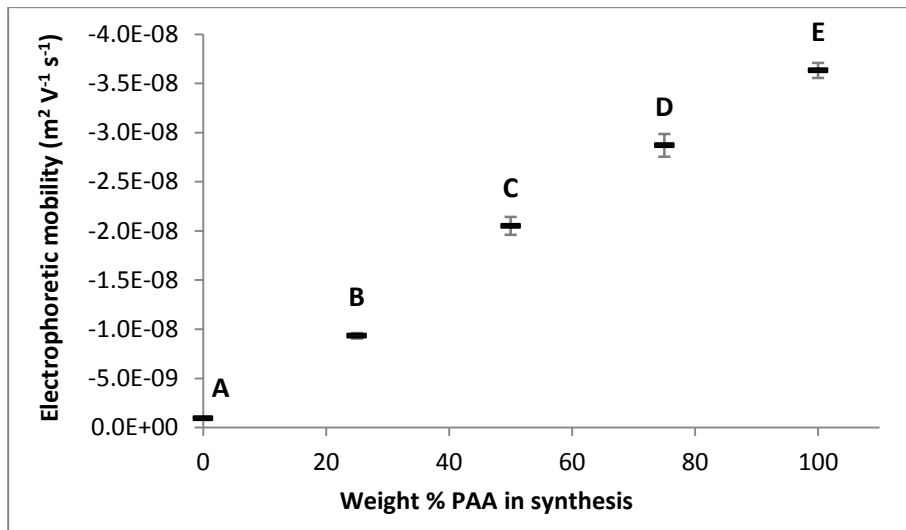
Figure 12. Electrophoretic mobility of particle type II, A–E; error bars show standard deviation[73]

4 The influence of particle charge on filter cake properties

In dewatering and filtration applications where filter cakes form, the filter cake properties will be the determining factor in the performance of the process. As mentioned previously in section 0, the properties of filter cakes made from organic matter differ markedly from those made from inorganic material.

4.1 The filtration process

Dead-end filtration experiments were carried out for both particle type I and II, using a piston–cylinder based dead-end filtration cell, Figure 13, developed in our laboratory [30,73,74].
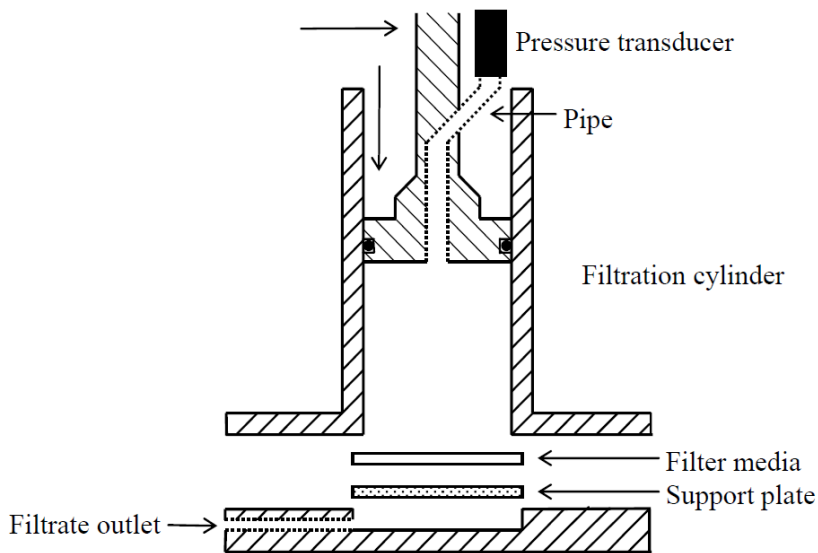
Figure 13. Schematic of the filtration setup (cylinder and piston. [30,73]

The filtration cylinder and piston used for the dead-end filtrations consisted of a 116-mm-high cylinder with a bore diameter of 22 mm for filtration of type I particles and 50 mm for filtration of type 2 particles, fitted with a piston with a pneumatic piston seal. The liquid pressure was measured at the piston/water interface by a pressure transducer connected through a pipe and logged along with applied pressure, piston displacement, and filtration time in a data file. To prevent

evaporation through the filter medium during the filtration experiment, the base incorporated a collection chamber under the filter medium, connected via a pipe to a beaker, while the filter medium itself, placed between the cylinder and the base, also functioned as a seal between the two parts. All filtration experiments were completed at high pH (above 9) to ensure full deprotonation of PAA [30,73].

The filtration/dewatering process can be divided into two distinct phases. In the filtration phase, the piston drives the suspension against a filter medium on which the solids are deposited while the liquid is expelled. As the settling velocity of these particles is very low compared to the duration of the filtration, particle settlement is ignored and it is assumed that the suspension above the filter cake is homogeneous throughout the entire filtration process. This will cause the filter cake resistance will increase over time, as the filter cake grows, while the average specific resistance should be constant at constant pressure, assuming filter resistance to be negligible as well as a linear increase in solid pressure with position, down through the filter cake, which has been proven to be the case for other synthetic particles [47]. Once the piston face touches the filter cake, a transition between the filtration and consolidation phases occurs. Starting from this point, the solid pressure in any part of the filter cake approaches the value of the applied pressure. The solid density will at first homogenize throughout the filter cake, expelling the water in the pores (primary consolidation); after a while, the particles in the filter cake will begin to rearrange and in some cases even deform and compress (secondary consolidation) [75]. At the end of the consolidation process, the filter cake cannot compress any more, as the applied force equals the inter-particular forces and thus no more water can be expelled. The onset of the consolidation phase is seen as a sharp decrease in both liquid pressure and permeate flux, as illustrated in Figure 14 [30].
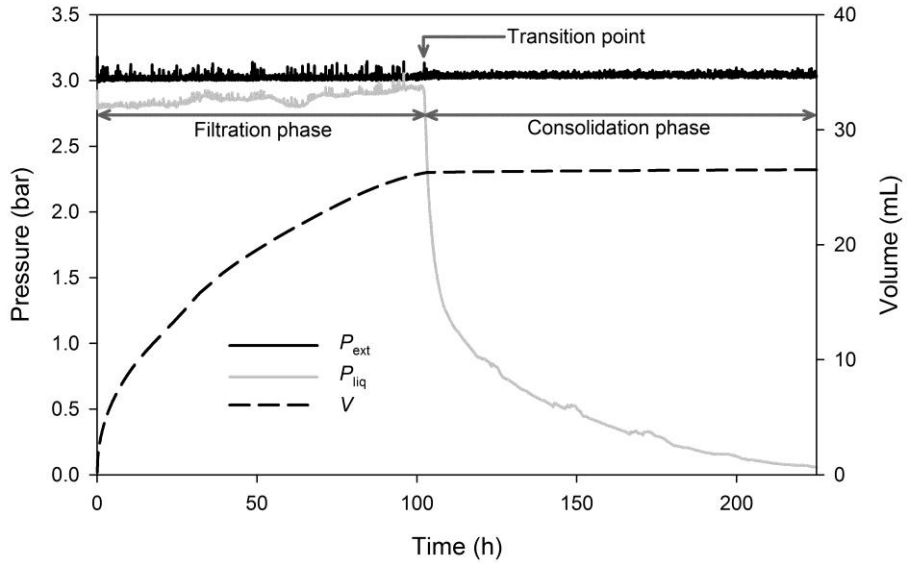
Figure 14. Applied (P_{ext}) and liquid (P_{liq}) pressures along with the filtrate volume (V) as functions of filtration time for PSA 67/0 (type I) at 3 bar. Arrows show the filtration and consolidation phases and the transition point between the two [30]

4.2 Specific filter cake resistance

Data obtained during the filtration phase was analyzed using a modified version of Darcy's law of flow through a porous medium, shown in eq. 5 [76]:

$$\frac{t}{V_f} = \frac{\mu\,\hat{\alpha}\,s}{2P_{eff}A^2}V_f\Bigg|_{P_{eff}=P_{app}-\Delta\pi} \qquad\qquad \textbf{\textit{Eq. 5}}$$

where t is time (s), V_f the filtrate volume (m^3), μ the filtrate viscosity (Pa s), A the filter medium area (m^2), P_{eff} the effective liquid pressure – also denoted P_{liq} (Pa) (corresponding to the applied pressure, P_{app} - also denoted P_{ext}, minus the osmotic pressure in the filer cake, $\Delta\pi$), s the amount of dry matter deposited in the filter cake per volume of filtrate (kg m^{-3}) (or simply the dry matter content of the suspension to be filtered, if the suspension is dilute and all dry matter is retained, as it is in this case), and $\hat{\alpha}$ the average specific filter cake resistance (m kg^{-1}). Membrane resistance is negligible compared with the filter cake resistance and can be ignored. $\hat{\alpha}$ can then be calculated from the slope of a of a $t\,V^{-1}$ vs. V plot. Such a plot is shown as examples for both type I particles (Figure 15) and type II particles (Figure 16),

35

where the dashed grey lines are the linear fit used to obtain the slope. In Figure 15, a small "kink" is seen approx. halfway through the filtration due to unknown and unexpected events occurring during filtration. This has also been observed during the filtration of other type I particles, especially for PSA 74/0 at 3 and 4 bars. The implications of this is discussed more in-depth in supporting paper I [30]. This is not the case for particle type II, (probably due to lower concentration and shorter filtration times), but instead, filter cake resistance is not noticeable before approx. 10 % of total filtrate volume has passed the membrane, corresponding to approx. 3 layers of particles.
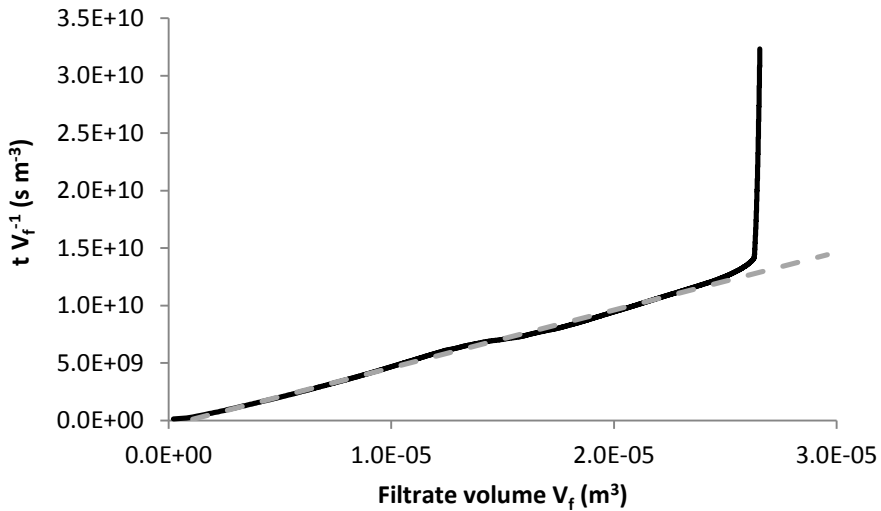
Figure 15. Example of a t V^{-1} vs. V plot for particle type I (PSA 67/0) at an applied pressure of 3 bar. Dashed line show the linear fit, the slope of which is used to calculate α [30]
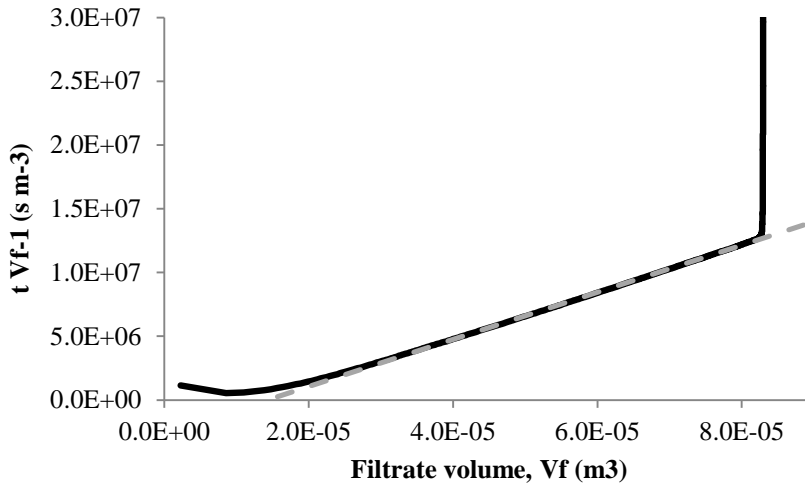
Figure 16. Example of a t V^{-1} vs. V plot for particle type II (C) at an applied pressure of 1 bar. Dashed line show the linear fit, the slope of which is used to calculate α [73]

In all cases, the specific cake resistance was found to increase with particle charge, as shown in Figure 17, where resistance increases with shell to core ratio, and Figure 18, where the direct influence of charge is seen. There was, however, an observed difference, between the particle types, in how the resistance depends on pressure. For type I, specific resistance increase linear with increasing pressure (2-6 bars), whereas this is not true for type II. In the latter case, the nonlinear response of resistance on pressure (0.1-1 bar) was found to be large at the low end of the pressure range and small at the high end, seemingly approaching a limiting value. It is not possible to make a direct comparison of the two experiments, due to the difference pressure ranges and the nature of the particles, but it can be concluded that both particle types formed compressible filter cakes, with the compressibility increasing as particle charge increase.

Figure 17. Specific filter cake resistance as a function of applied pressure, for particle type I. Values for PSA 74/0 at 3 and 4 bar are considered outliers [30]
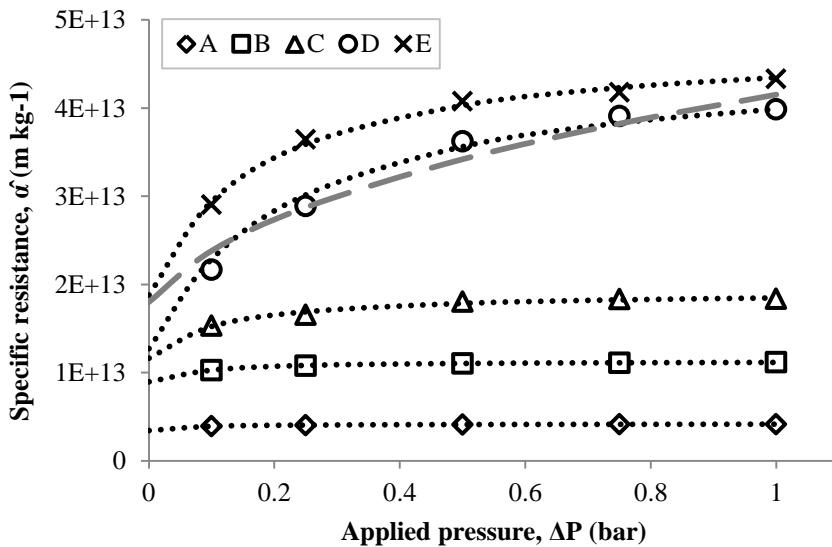
Figure 18. Specific filter cake resistance as a function of applied pressure, for particle type II. Dotted lines show the model from eq. 7, while the dashed line show the model from eq. 6 [73]

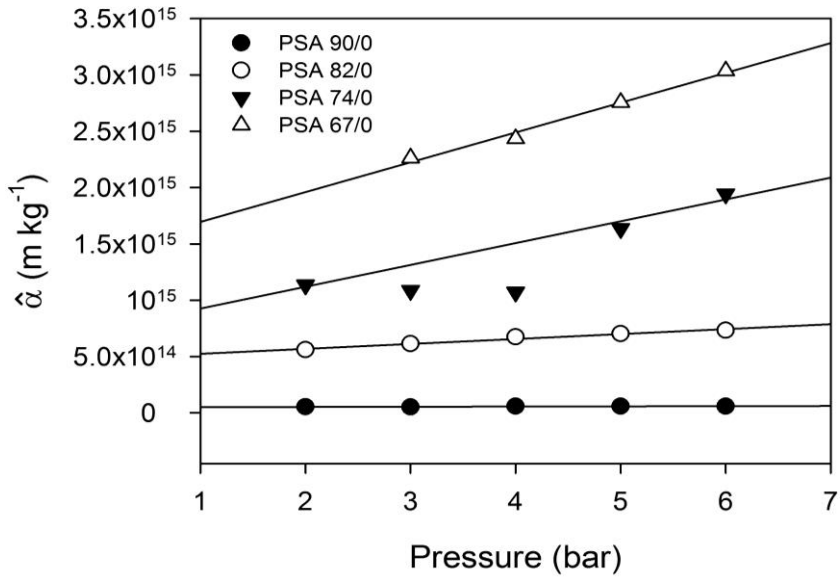The linear dependency between pressure and specific resistance, found for particle type I, is also an often observed feature in wastewater sludge filtration [22,28,36,77], where the relationship between specific resistance and pressure follows the model developed by Tiller [28,29], eq. 6. Here α_0 is the apparent zero-pressure resistance, while P_a and n are empirical parameters related to cake compressibility. For highly compressible filter cakes, as in this case, $n = 1$ to give a linear expression.

$$\alpha = \alpha_0 \left(1 + \frac{P_{liq}}{P_a} \right)^n \qquad\qquad \textbf{\textit{Eq. 6}}$$

From this we get the values of $\hat{\alpha_o}$ and Pa presented in Figure 19, which clearly shows the influence of shell thickness on both resistance and compressibility (right) as well as charge density in the pores, here shown as gel concentration (left). The result in Figure 19, right is in good agreement with the work of Johnson & Deen [78] on the permeability of agarose gels, in which he found an inverse relationship between permeability and polymer concentration in the gel. These findings reduce the importance of porosity, viewed in the classical sense as the void between particles, but increase the importance of the gel density in the inter-particle space in the filter cake [30].
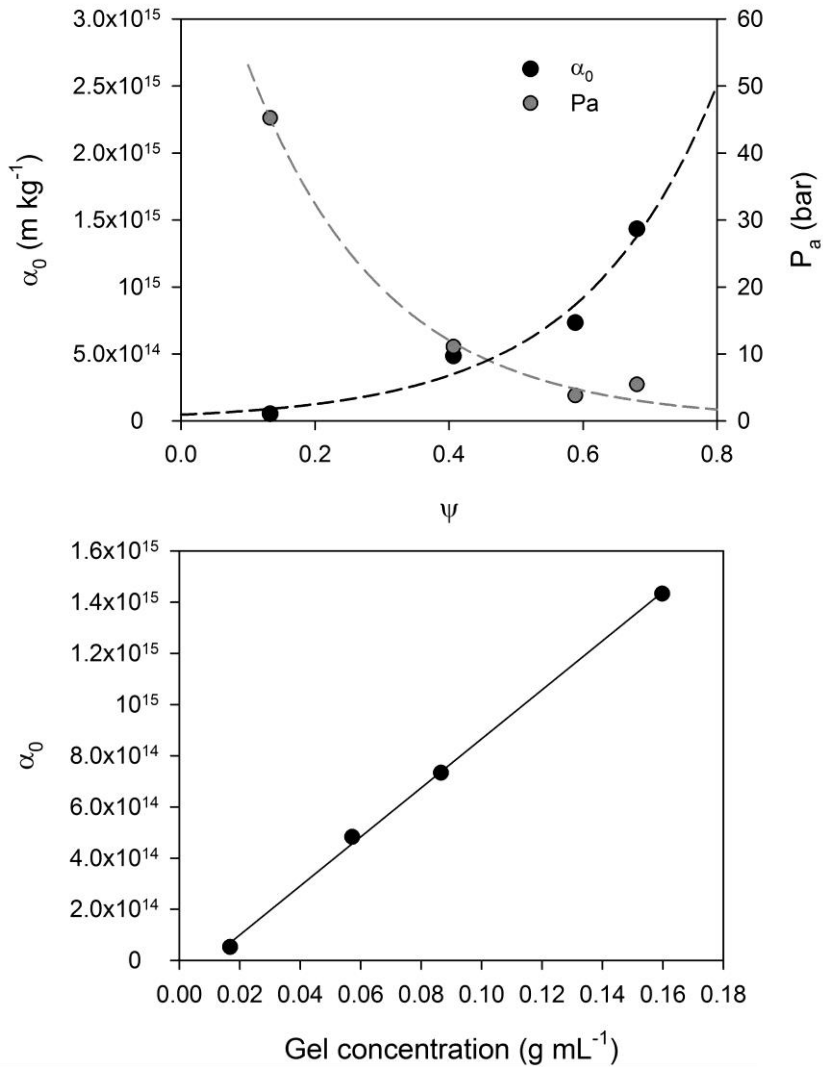
Figure 19. Influence of shell to core ratio of particle type I on α_0 and P_a (top) and gel concentration in the pores (partly due to deformation and overlapping) on α_0 [30]

This was, however, not the case for type II particles. In this case, the nonlinear response of resistance on pressure (0.1-1 bar) was found to be large at the low end of the pressure range and small at the high end, seemingly approaching a limiting value. Attempts to use eq. 6 on type II particles did not provide a good fit to the data. An example of this is shown in Figure 18 as a dashed grey line. Instead a new

empirical model is proposed, eq. 7, to give a better fit to the experimental data. In this model, b and K are fitting parameters while $\hat{\alpha_0}$ has the same definition as in eq. 6. The true maximum specific resistance, $\hat{\alpha_{max}}$, (at high pressure) is then the sum of α_{0_s} and b. Filter cake compressibility is evaluated from K and b, with K determining the filter cake compressive strength (high K = high strength), i.e., the response to changes in pressure, while b determines the magnitude this has on changes of $\hat{\alpha}$. The expression, $b/(1+K)$, is thus useful in determining the compressibility in terms of resistance [73].

$$\hat{\alpha} = \frac{P_{liq}b}{P_{liq} + K} + \alpha_0 \qquad\qquad \textbf{\textit{Eq. 7}}$$

Even though this model does fit the data very well in the range between 0.1 and 1 bar (dotted black lines in Figure 18), it is difficult to say if it is accurate below 0.1 bar, as no experimental data is available in this range [73]. Despite of this, data from the model is used in the determinations of $\hat{\alpha_0}$ and filter cake compression, presented in the discussion section, and these data should be evaluated with the high degree of uncertainty in mind. In Figure 20, the resulting values of $\hat{\alpha_0}$ and compressibility are presented, which, as in the case of particle type I, also show both resistance and compressibility to increase with particle charge, here presented as zeta-potential.

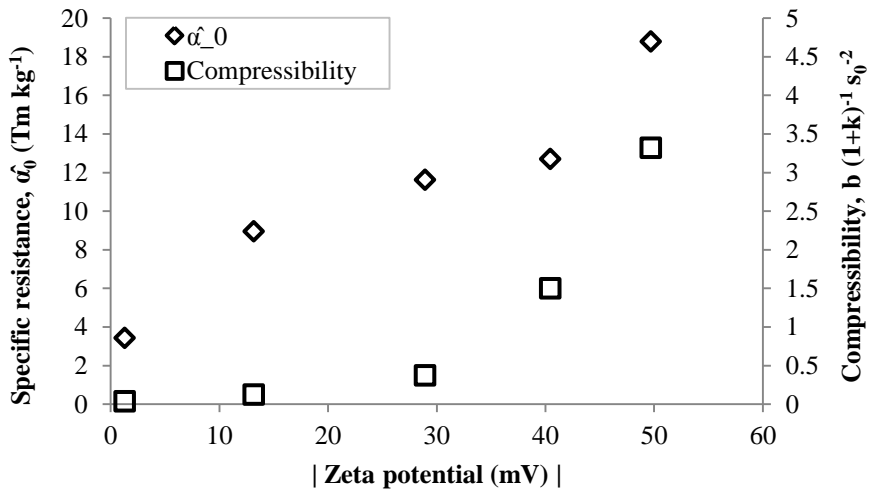***Figure 20. Influence of particle zeta potential on α_0 and compressibility [73]***

Even though is not possible to make a direct comparison of the two experiments, due to the different pressure ranges and the nature of the particles, it can be

concluded, that both particle types formed compressible filter cakes, with the compressibility increasing as particle charge increase.

4.3 Consolidation

At the end of the filtration phase, i.e., when the piston touches the top of the filter cake, consolidation will begin. Also here, the two particles types show a distinct difference in behavior. Particle type I facilitated both primary and secondary consolidation of the filter cake, with secondary consolidation becoming more dominant as the shell volume ration increases [30]. The degree of consolidation, $U(t)$, is defined by eq. 8 [75].

$$U\left(t\right)=\left.\frac{V\left(t\right)-V_{tr}}{V_{\infty}-V_{tr}}\right|_{V(t)\geq V_{tr}} \qquad\qquad \textbf{\textit{Eq. 8}}$$

Here $V(t)$, V_{tr}, and V_{∞} are the filtrate volume expelled at time t, at the transition point, and at equilibrium, respectively. Thus, V_{∞} is the filtrate volume measured at the end of the experiment, when no more water can be expelled from the filter cake. In this case, the transition point and thus also V_{tr} is determined from the liquid pressure measurement, when a large drop is observed in the liquid pressure, as illustrated in Figure 14 [79]. The degree of consolidation for PSA67/0 at 5 bar is shown in Figure 21 as a function of the square root of time. At U<0.2, the cake undergoes primary consolidation, after which secondary consolidation takes over, as evident from a decrease in the slope of the plot. All the remaining consolidation plots have the same general appearance with the two consolidation phases clearly distinguishable [30].
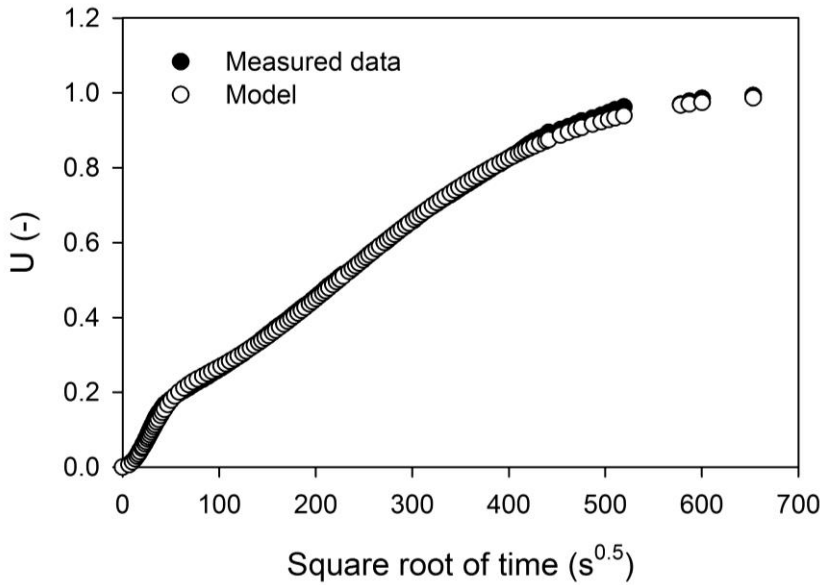
Figure 21. The degree of consolidation as a function of the square root of time for PSA 67/0 at 5 bar. Modelled data are discussed in supporting paper I [30]

The consolidation of particle type II was much faster than for type I and did only display primary consolidation, as shown in Figure 22.
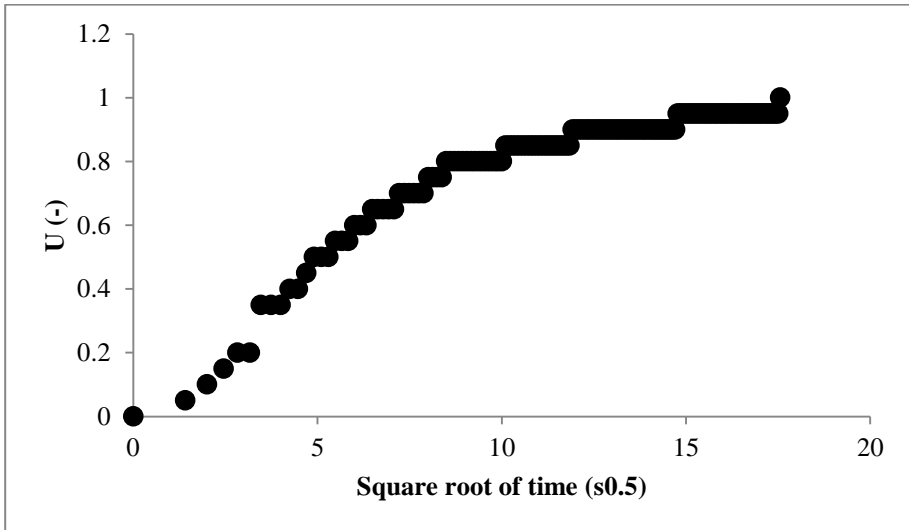
Figure 22. The degree of consolidation as a function of the square root of time for particle D at 1 bar

This difference is attributed to the lower shell to core ratio for particle type II and the fact that the lower filtration pressures, used for this particle type, is not enough for cake porosity to reach a value low enough for creep effects to occur.

4.4 Porosity

Filter cake porosity was determined at the transition between filtration and consolidation for particle type I and at the end of consolidation for both particle types.

For particle type I, the dry matter content of the filter cake was evaluated gravimetrically by letting a sample of the filter cake dry for at least 24 h at 104°C. The dry matter content of the filter cake after complete consolidation was higher than at the transition point, and neither displayed any correlation with the applied pressure. However, the dry matter content of the filter cakes is weakly correlated with ψ, as shown in Figure 23, where a larger shell to core ratio resulted in a lower dry matter content [30].
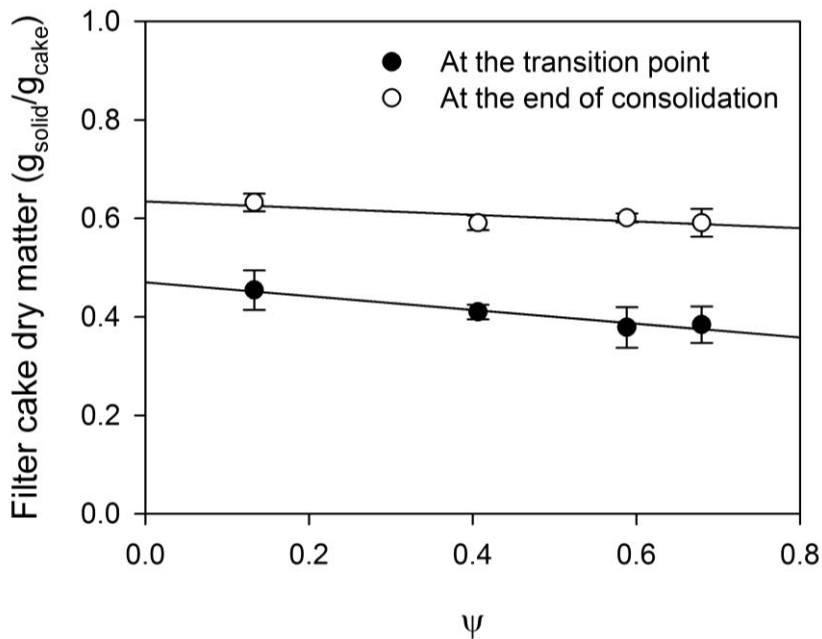
Figure 23. The dry matter content of the filter cakes as a function of shell to core ratio (ψ). Values are presented as average values over the different applied pressures, with error bars showing the standard deviation [30]

As mentioned earlier, the density of the PSA particles is very close to that of water, thus the solid volume fraction, or solidosity, of the filter cake, Φ (=1-ε), is approximately equal to the dry matter content of the filter cake. The solid volume fraction of the filter cake can also be given by eq. 9, where Φ_{pack} is the packing fraction of the swollen particles and Φ_{col} is the solid volume fraction of a single particle, which equals $1 - \psi$ for fully swollen particles [30].

$$\Phi = \Phi_{pack} \cdot \Phi_{col} \qquad\qquad Eq.\ 9$$

In the case of no deformation, overlapping, or compression of the water-swollen shell, the absolute maximum packing fraction cannot exceed 0.74 (hexagonal close-packed spheres (HCP)). Under these conditions, Φ would be approx. 0.2 for PSA67/0, which is much smaller than the measured value, and it can be inferred, that the shells must deform and/or overlap for Φ to increase above 0.2. Again using eq. 9, it is possible to calculate Φ_{pack} from experimental data and compare this to the deformation limit and the overlapping limit (assuming that deformation occurs much more easily than overlapping). For this, the deformation limit is set to 0.625 (random close packed) and the overlapping limit to 1 (the point where there is no more free pore space for the shell to occupy). [30]

Figure 24. Apparent values of $\phi_{packing}$ for the four batches of PSA particles at the transition point and at the end of consolidation [30]

The result is shown in Figure 24 and can give an idea of how the shells will deform and overlap/compress during filtration and consolidation. Deformation already occur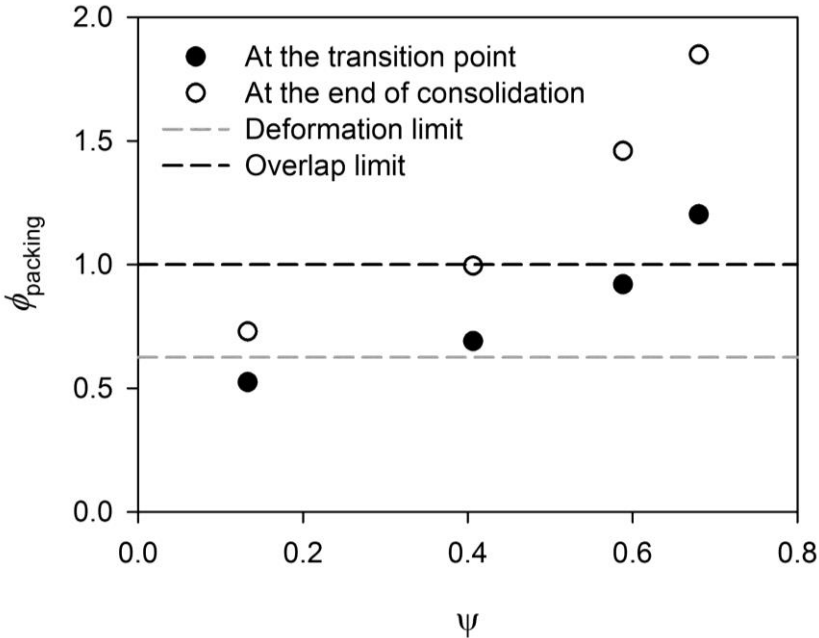s during the filtration phase for all classes of particle type I, apart from the one with the smallest shell fraction. The observed increase in the pressure dependency on $\hat{\alpha}$, shown in Figure 17, might then be explained by less energy being required to overlap or compress the shells at a high shell to core ratio. Even though the gel-filled pores, at the overlap limit, are larger for particles with a high shell to core ratio, (increasing ψ lowers the solidosity), the concentration of gel in the cake seems to have an even greater effect on the specific cake resistance, underlining the strong dependency of resistance with gel concentration, (Figure 19, bottom) [30].

For particle type II, porosity was obtained using a pressure step experiment within the same pressure range as used during the filtrations and evaluated from piston position, i.e., cake volume, instead of gravimetrically [73]. This method was chosen due to the liquid nature of the filter cake (the cake swelled when the piston was removed), which made retrieval of the consolidated cake impossible. The volume of the wet filter cake, V_c at the different pressure equilibriums was calculated by subtracting the filtrate volume, V_f and the volume lost in the tubing, V_{loss} from the initially added volume, V_{init}. V_c is then used, along with the total mass of the deposited particles to determine the filter cake porosity, $\varepsilon = 1 - \phi$ after consolidation based on eq. 10 [73].

$$\Phi = \frac{\left(V_{init} - V_{loss}\right)s}{V_c \rho_p} \quad ; \quad V_c = V_{init} - V_{loss} - V_f \qquad \textbf{\textit{Eq. 10}}$$

It is assumed that the cake is fully consolidated, i.e., the porosity is uniform throughout the cake. This allows the use of eq. 11 [28] for relating solidosity, ϕ with solid pressure, P_s (where $P_{app} = P_s$ when the cake is fully consolidated), as the local porosity equals the average porosity, in this situation, and thus can be used interchangeably. Analogue to eq. 6 and 7, ϕ_0 is the solidosity at the zero-pressure limit and β and P_a are empirical parameters related to cake compressibility.

$$\Phi = \Phi_0 \left(1 + \frac{P_s}{P_a}\right)^{\beta} \qquad \textbf{\textit{Eq. 11}}$$

This model proved to be an exceptionally good fit, fitting parameters listed in Table 3, where most notably β is within the range found in compression experiments of biological suspensions [28]. ε_0 is difficult to compare as most suspended material of organic biological often is characterized by a high volume fraction of water inside the actual particles/cells and/or trapped between aggregated particles as interstitial water. This would, depending on how porosity is measured, lead to assumptions of a

pore volume larger than the actual volume available for flow in the cake, which in turn leads to a very high porosity. This is not the case in this work, as the particle core does not swell in water. P_a is also well above the range normally encountered for biological material, but as P_a and ε_0 is correlated, and ε_0 is high for reasons mentioned above, a direct comparison with biological material would not be meaningful. There is, however a clear dependence on all parameters of particle charge, showing that charge does play a big role in the compression of the filter cake [73].

Table 3. Fitting parameters obtained from the fitting of eq. 11 to experimentally obtained data of filter cake porosity [73]

Particle ID	ε_0	P_a (bar)	β
A	0.590	1.303	0.643
B	0.602	1.181	0.576
C	0.615	1.060	0.508
D	0.624	0.911	0.436
E	0.642	0.724	0.360

Figure 25 shows the obtained porosities as well as the fitted model from eq. 11 (dashed/dotted lines). A distinct increase in porosity was observed as particle charge increase, but unlike particle type I, an increase in applied pressure facilitated a compaction (or physical compression) of the filter cake, leading to lower porosities. This also had the effect of doubling the difference in porosity between the charged and uncharged particles, as particle charge served to decrease the physical compressibility of the cake, in sharp contrast to the relation between pressure and resistance.
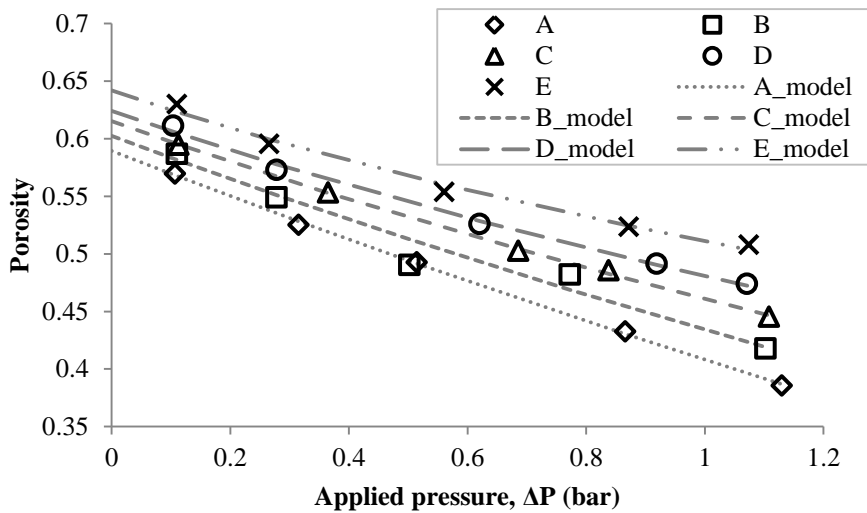
Figure 25. Filter cake porosity as a function of applied pressure. Dashed/dotted lines show the model from eq. 11 [73]

This discrepancy becomes very clear when directly comparing porosity with specific resistance, the result of which is shown in Figure 26. Here it becomes evident, that the effects of particle charge significantly outweighs the effect of porosity, even at low porosity values [73]. Please note, that the measured specific resistances has been divided by the square of the volume specific surface area of the particles, s_0^2, to eliminate any effect caused by differences in particle size (Particle E is bigger than the rest).
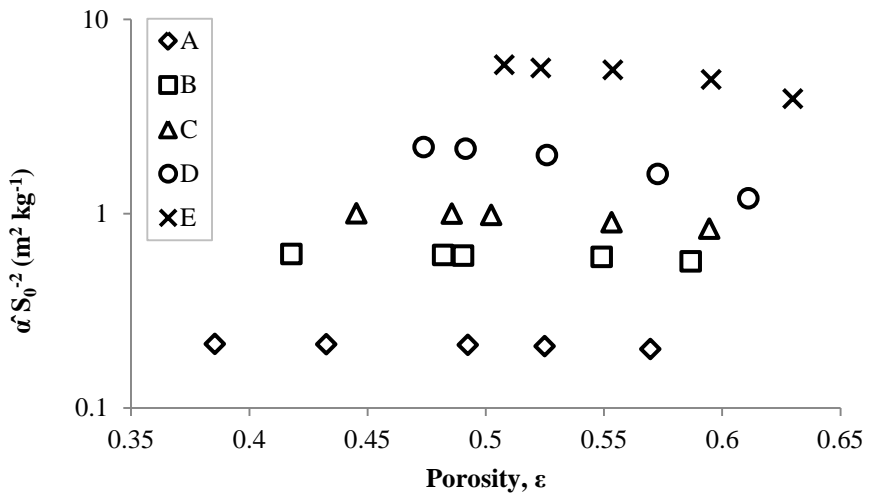
Figure 26. The influence of porosity on specific resistance, α, taking particle size into account. Note log-scale on y-axis [73]

5 What's the deal with all these charges?

As presented in the previous 3 sections, particle charge seems to have a pronounced effect on all the investigated properties of the filter cake. The obtained values of specific resistance was compared to empirical models, showing that the models severely underestimates the resistance as particle charge increase, while providing a reasonably good fit in the case of no particle charge [73]. For particle type I, it was also shown, that doubling particle size did not have a significant effect on filter cake resistance [30]. Combined with the fact that there is a discrepancy between the influence of increased particle charge on porosity and on resistance (they both increase, which is contradicting), this show that cake filtration is much more governed by particle charge than by cake structure.

As the cake is compressed, the particles move closer to each other until the outer force (the applied pressure) equals the interparticular forces. If looking solely on the charge effect, charged particles will repel each other due to electrostatic interactions, while an increased osmotic pressure will occur due to the presence of counter ions. Depending on particle type, there will also be other repulsive forces between the particles, such as steric hindrance, caused by the principle of excluded volume, which is discussed later. For particle type I, the large relative volume of the shell and the high pressures used during filtration, causes the shells to deform and/or overlap during filter cake compression. The pores would then become full of a polyacrylic acid gel, which would assert added hydraulic resistance and increased osmotic pressure.

For this type of particle, the amount of charges in the shell increase with shell volume, but the concentration remains constant, as seen in Figure 27, that shows an almost linear correlation between amount of carboxylic acid groups and shell volume.
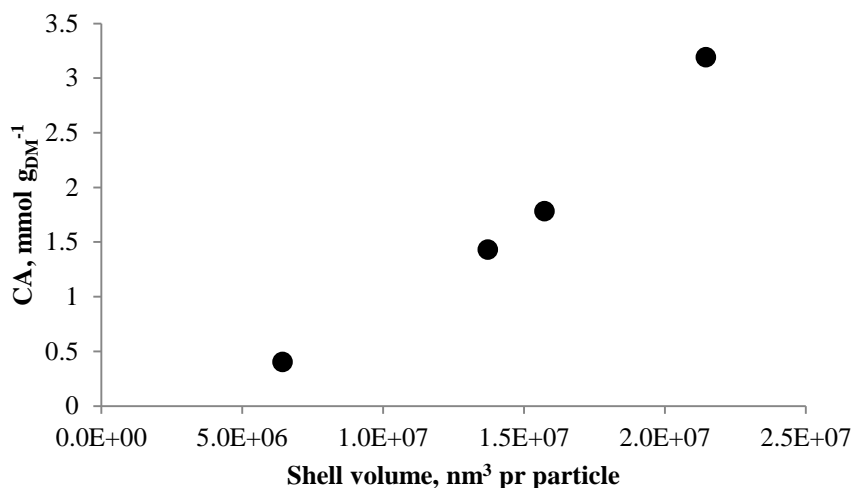
Figure 27. Amount of carboxylic acid groups found (by titration) per shell volume

This would presumably cause the grafting density to be equal for all type I particles, only varying the length of the PAA chains. As the particles are spherical, the increase of the shell thickness, along with the decrease in core diameter would cause the distance between the polymers in the outer layers of the shell to be larger for particles with a high value of ψ. This would cause the surface charge density (charge per surface unit) to be highest for small values of ψ and lowest for high values of ψ. Indeed, estimations based on particle size, shell volume and number of carboxylic acid groups (by titration), show the grafting density of PSA 67/0 (high ψ) to be half of that of PSA 90/0 (low ψ). As the electrostatic repulsion depends on this surface charge density, a higher degree of deformation/overlapping would be possible for the large shell particles. Furthermore, the lack of any correlation between porosity and applied pressure, suggests that osmotic pressure is not the limiting factor in terms of cake compression. Instead, it is thought, that compression I limited by mutual volume exclusion of the polymers in the shell as they overlap, i.e., two segments of polymer cannot occupy the same space at once, as well as reptation of the polymers during secondary consolidation, which is more dependent on time and less on pressure [30]. If the particles are assumed to be arranged in a hexagonal close packed (HCP) structure, a detailed discussion of which can be found in supporting paper III [73], the interparticle distance, L, can be calculated from eq. 12, based on simple geometric considerations and knowledge about the solid and liquid volume fractions of such a structure [73,80]. Here R is the radius of the particles, which in this case will be the particle core.

$$L = 2\left(\frac{0.904R}{\sqrt[3]{1-\varepsilon}} - R\right) \qquad\qquad \textit{Eq. 12}$$
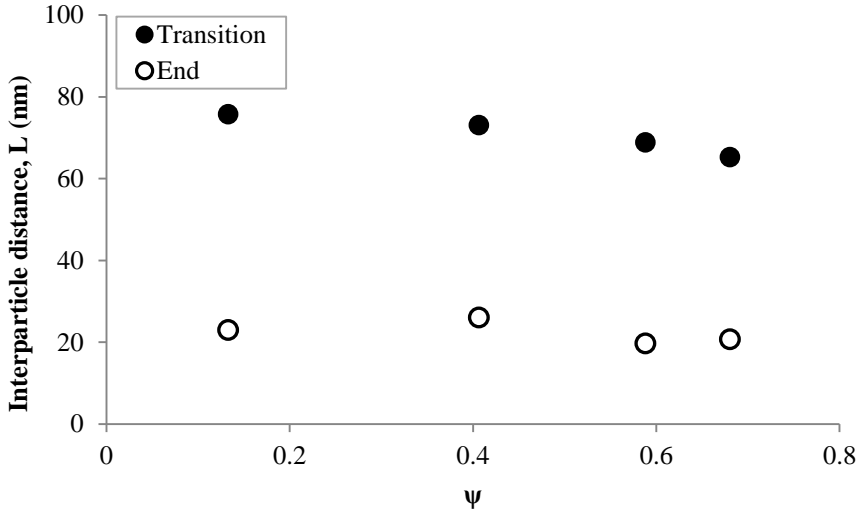
Figure 28. Calculated interparticle distance as a function of shell to core ratio at the transition point and at the end of consolidation

From Figure 28 it can be seen, that there is only a small difference in the distance between the particle cores, both at the transition point and at the end of the consolidation. This confirms the notion, that the separation of the particles are limited by mutual volume exclusion of the shell polymers, i.e., the shells can overlap, as long as there is available space for one polymer to fit between two others, as sketched in Figure 29, where the black lines indicate a grafted polymer and the grey area around the lines indicate the excluded volume, i.e., space than cannot overlap with another polymer or another polymers excluded volume.
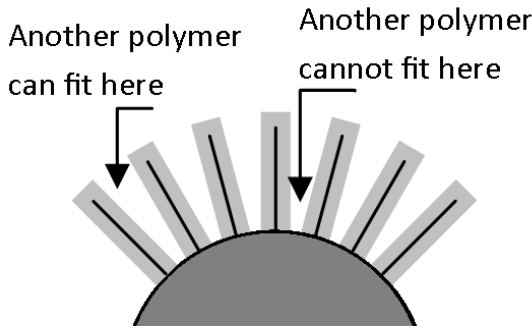
Figure 29.Over-simplified schematic of attached polymers on particles surface, showing the concept of excluded volume

This is however not the case with particle type II, due the high porosities in the charged filter cakes made from these particles. Based on the same assumptions as before, calculated pore size, eq. 13, and interparticle distance, eq. 12, suggest the pores to be too big and the particles to be too far apart for the classical interpretation of the DLVO theory to have any appreciable effect on resistance [73]. Assuming HCP structure and using data obtained at 1 bar external pressure, pore diameter increases from 390 nm to 710 nm, going from low to high charge, while interparticle distance increases from 86 nm to 320 nm, both of which is well above the double layer thickness.

$$d_p = 2\left(\frac{(2R + L) \cdot \mathrm{Sin}(30)}{\mathrm{Sin}(120)} - R \right) \qquad \textit{Eq. 13}$$

However, recent works have found the classical DLVO theory to break down in systems where charged colloids are confined between charged walls or within charged pores, proposing an increased distribution of counter ions to be the cause [81–83]. In all instances, the interparticle distance was found to be larger than shell thickness, indicating that there should be no appreciable deformation and/or overlapping of the shells, therefore the gel-in-pore effect, discussed for particle type I, will not be present here. Following the circumstances mentioned above, osmotic pressure is assumed to be the primary reason for the observed high resistance [73]. Under this assumption, and since the specific cake resistance of non-charged particles (particle A) seems to fit well with empirical models, it is possible to calculate P_π for particles B-E (osmotic pressure counteracts the applied pressure causing the effective pressure to diminish, as proposed by Keiding and Rasmussen [37] and noted in eq. 5). The result of this is shown in Figure 30, as a function of porosity, with osmotic pressure increasing both with particle charge and with decreasing porosity (smaller pore volume = higher counter ion concentration).
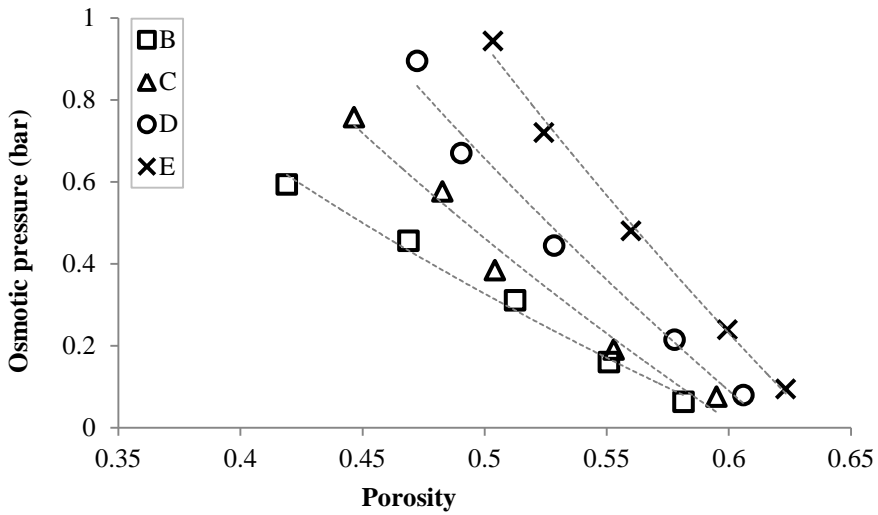
Figure 30. Calculated osmotic pressure in the pores as a function of filter cake porosity [73]

Based on a grafting density of PAA to the particle surfaces of $5.7 \cdot 10^{15}$ grafts per square meter (determined theoretically in supporting paper III [59]), it is possible to calculate the maximum concentration of counter ions in the pores (assuming all the available counter ions are distributed evenly in the pore volume). The ratio between this value and the concentration needed to achieve the previously determined osmotic pressure are presented in Figure 31. In almost all instances, this ratio is above 1 (dotted line), indicating that the notion of osmotic pressure in filter cakes, might be a valid explanation for the observed high values of α often found during filtration of wastewater sludge and other suspensions of biological origin. Ideally, the ratio should be 1 for all porosities, but as this is based on evenly distributed counter ions, which is not necessarily the case, all counter ions might not be osmotically active at higher porosities.
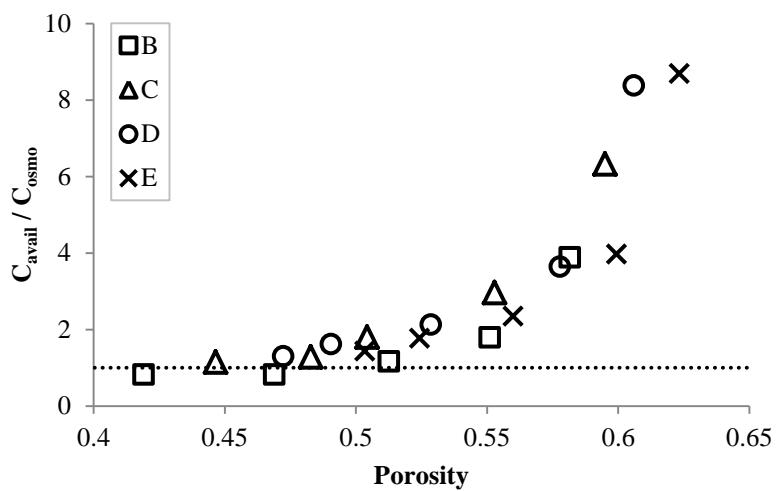
Figure 31. The ratio between concentration of available counter ions from PAA and the concentration needed to for the calculated osmotic pressure – dotted line inserted at a 1:1 ratio [73]

6 Direct observation

Supplementing the dead-end experiments, direct visual observations of the filtration process offered a promising alternative in studying filter cake behaviour. By using this method, the filter cake can be monitored in real-time, using an image recording device (an HD video camera in this case) attached to the viewing port of an optical microscope. The focus of the microscope was adjusted to give a clear tangential view, orthogonal to the length of the membrane, as illustrated in Figure 32, which also shows the direction of the different flows. For these experiments, a third set of particles where used, similar to type II, but bigger to allow better visualization. The filtration was done in cross-flow mode, using a specialized filtration cell, containing just a single hollow fibre membrane. A detailed description of the setup and experimental conditions are available in supporting paper IV [11].
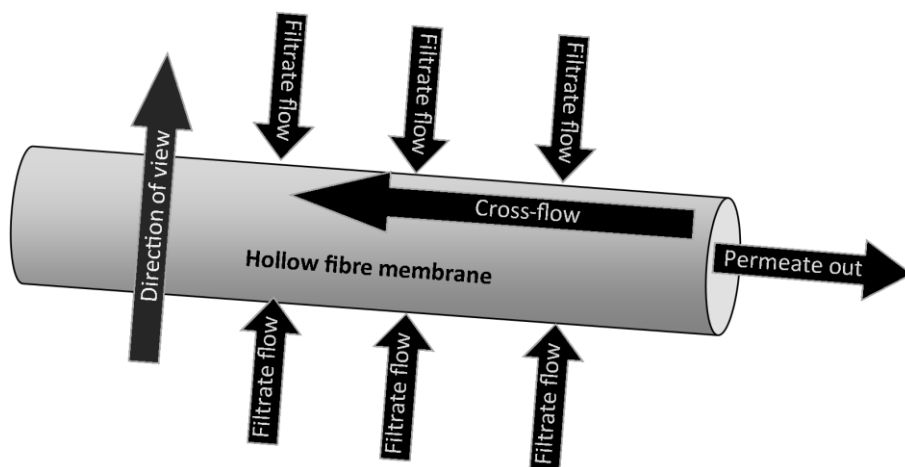
Figure 32. Shematic of the hollw-fibre used in the direct observation experiments, along with flow directions

The resulting pictures display the membrane surface as dark and the background as bright. Due to refraction, the particles appear bright in the middle with a dark edge (only at high magnification) and the filter cake generally appear dark, similar to the membrane. An example of the growth of a filter cake is shown in Figure 33, for a constant flux filtration over the course of 4 hours, with the interface between the membrane and filter cake being indicated by a dashed white line [11]. By using a microscopic scale along with an image analysis tool, the cake height is easily determined
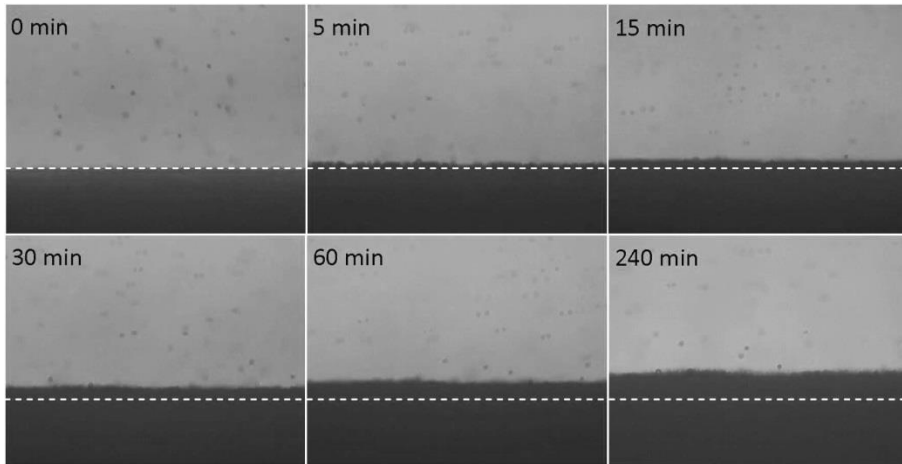
Figure 33. Evolution of filter cake height during constant flux for 4 h [11]

During cross-flow filtration suspended material is continuously drawn towards the membrane due the convective flow. The cake growth rate was calculated from eq. 14 as the growth obtained in μm per mL of permeate passing through the membrane, where h_{cake} is the cake height, V_{perm} is the accumulated permeate volume, t is time and Q_{perm} is permeate flow rate. The resulting growth rates, for filtration at constant permeate flux, is presented in Figure 34, which shows, higher surface charge to generally result in a slower growing filter cake that also reaches a steady-state thickness more quickly [11].

$$v_{cake} = \frac{dh_{cake}}{dV_{perm}} = \frac{dh_{cake}}{dt} Q_{perm} \qquad\qquad \textit{Eq. 14}$$
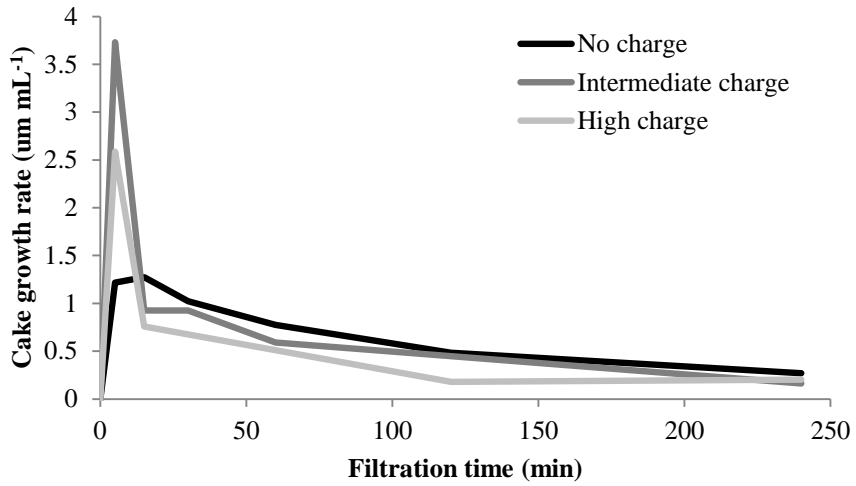
Figure 34. Filter cake growth rate at a constant permeate flux for high, intermediate and non-charged particles [11]

As the experiments did not provide data on cake porosity, cake thickness is used in evaluating specific resistance instead of cake mass, the result of which is shown in Figure 35.
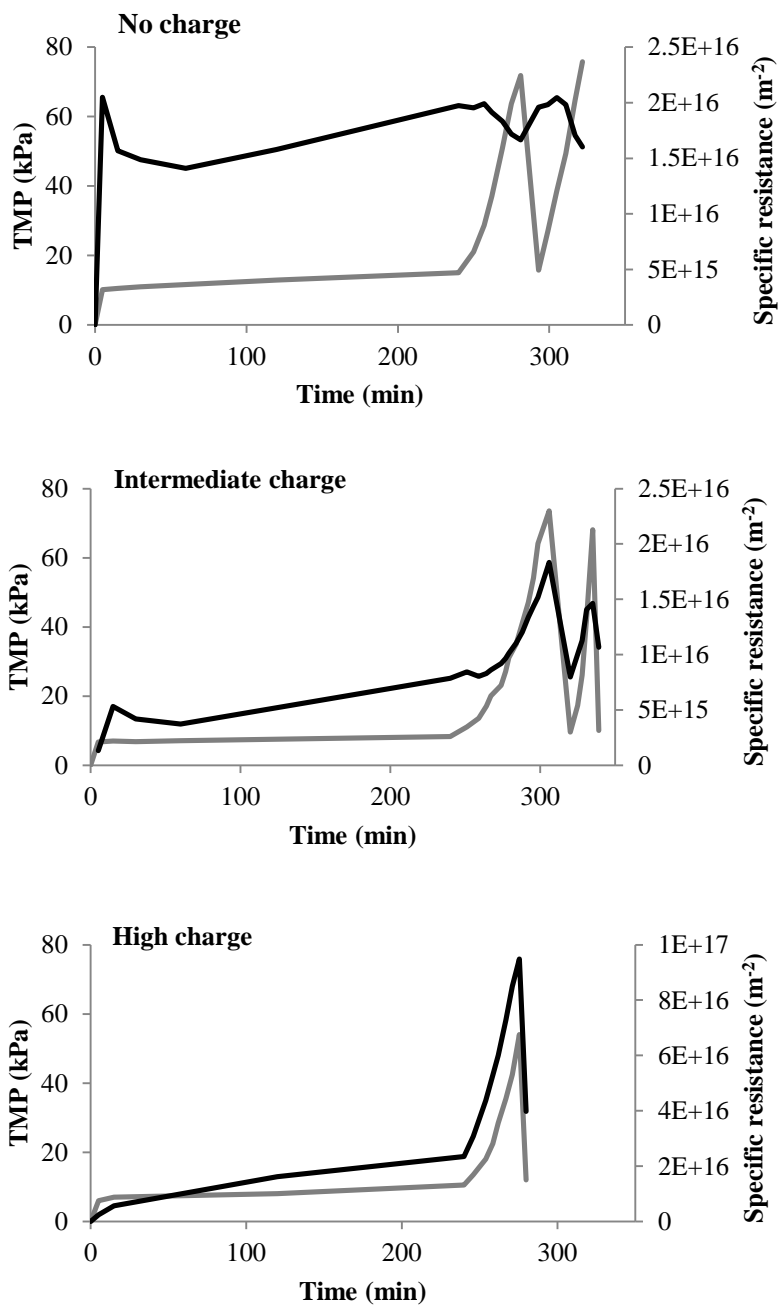
Figure 35. Specific cake resistance (black) and TMP (grey) for high, intermediate and non-charged particles [11]

60

For non-charged particles, the specific resistance (black line) increases only slightly during the course of the filtration, indicating that cake thickness is the main contributor to the increase in resistance over time. For highly charged particles, the specific resistance starts off comparatively low, only to increase by a factor of 10 during the initial cake build-up [11]. The low pressure during this phase must therefore be enough to facilitate some compression of the filter cake for this to happen. This compression is even more evident higher pressures, as the specific resistance increases sharply, while decreasing again when the pressure is lowered as well. The intermediately charged particles seem to behave like a mixture of these two extremes: This filter cake behaves almost like the cake of non-charged particles during the cake build-up phase, although with less specific resistance, but compresses at a higher TMP like the cake of highly charged particles, but to a smaller extent. Apart from the initially high resistance of the uncharged particles, this agrees well with the obtained results during dead-end filtration, especially in terms of compressibility [11].

It has previously been assumed, that the particles formed well-structured filter cakes (section 0), due to the interaction between the particles being predominantly repulsive [73]. By observing the movement of individual particles, as they deposit on the cake surface, this assumption can be strengthened. It was found, that the particles did not settle on first contact with the filter cake, but instead rolled along the cake surface until eventually settling in small depressions between other particles. This is exemplified in Figure 36, where the movement of a single particle is followed (white arrow) frame by frame, as it rolls along a monolayer of already deposited particles, while eventually disappearing as it settles in a dip.
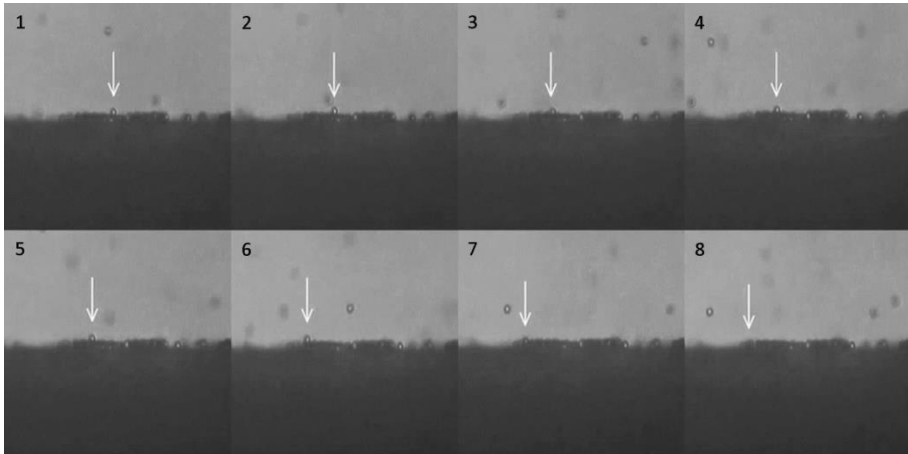
Figure 36. Formation of a monolayer of intermediately charged particles within the first minutes of filtration, and rolling of a single particle (white arrow). Black numbers show the sequence of the individual pictures [11]

Similar to this, the entire cake surface would roll as individual particles if pressure was relieved while maintaining cross-flow conditions. Here it should be noted, that the relation between cross-flow velocity and permeate velocity is approx. 3 orders of magnitude lower than normally found in cross-flow applications [84–86], as higher velocities will blur the image and make individual particle tracking impossible. This causes the cake to build faster, but should not have an impact on the cake structure, as the lateral movement of particles would only increase.

The method also showed compression and subsequent relaxation to be fast (within seconds) and reversible, while the degree of relaxation increased with particle charge. Figure 37 show the swelling of a filter cake made from intermediately charged particles over the course of 45 seconds. This underlines the notion of an increased osmotic pressure in the filter cake, due to the presence of counter ions associated with the charged surface (degree of swelling) as well as the lack of overlapping shells (fast swelling/compression). Implications of further relaxation, backwash and high shear are discussed in details in supporting paper IV [11].
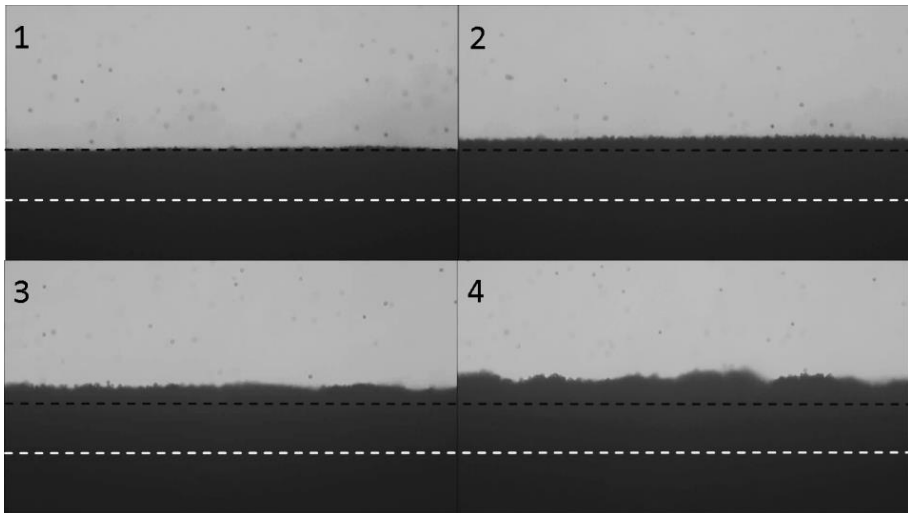
Figure 37. Swelling of a filter cake from intermediately charged particles with no cross-flow; Before swelling (1), after initial fast swelling, approximately 2 seconds (2), after 17 seconds (3) and after 45 seconds (4). The white line indicates the membrane–filter cake interface and the black line the filter cake–bulk interface before cake removal [11]

7 Conclusion

The aim of this PhD was to investigate the isolated influence of particle charge on filter cake behavior during filtration and dewatering. For this purpose, a range of novel model particles has been developed with the specific intent of controlling particle charge, while maintaining recumbence with particles found in activated sludge.

The main findings of this study are:

- Two classes of well-defined monodisperse core/shell model particles has been synthesized to mimic EPS covered sludge flocs and microbial cells. One with varying shell to core volume ratio, based on emulsifier-free emulsion polymerization and one with the novel ability to vary the surface charge density while maintaining a fixed shell to core volume ratio.

- For both particle types, surface charge has a pronounced influence on average specific cake resistance. In all instances, the resistance increases with charge with the resistance at the zero pressure limit being linear correlated with the total amount of charges present in the filter cake. Furthermore, compressibility, i.e., the dependency of pressure on resistance, was shown to also increase with charge.

- Comparison with empirical models, showed the models to severely underestimate the resistance as particle charge increase, while providing a reasonably good fit in the case of no particle charge.

- Consolidation was found to be slow for particles with a high shell to core ratio (creep effects are evident), but fast for particles with a low ratio. Furthermore, the ratio between secondary and primary consolidation increased with shell to core volume, while diminishing for particles with a fixed shell to core ratio, as they only experienced primary consolidation, regardless of charge density.

- For particles with a varying shell to core ratio, porosity was found to only increase slightly with shell to core ratio, while not being dependent on the applied pressure at all. This was ascribed to the high filtration pressures used for this particle type, causing enough physical compression for the cake to undergo secondary consolidation, which is less dependent on pressure. For a fixed shell to core ratio, surface charge density proved to have a significant influence on porosity, ranging from low for uncharged particles too high for highly charged particles. In this case, as the pressure increased, a compaction of the filter cake occurred, leading to lower

porosities. This also had the effect of doubling the difference in porosity between the charged and uncharged particles, as particle charge served to decrease the physical compressibility of the cake, in sharp contrast to the mentioned relation between pressure and resistance.

- It was found that particle size did not have a significant effect on filter cake resistance. This, combined with the fact that there is a discrepancy between the influence of increased particle charge on porosity and on resistance (they both increase, which is contradicting), show that cake filtration is much more governed by particle charge than by cake structure. In the case of a high shell to core ratio, this could be explained by the deformation and overlapping of the shells in a way that the pores would become full of a polyacrylic acid gel. For particles with a fixed shell to core ratio, calculated pore size suggest the pores to be too big for the classical interpretation of the electric double layer to have any appreciable effect on resistance. However, based on recent works that found the classical DLVO theory to break down in systems where charged colloids are confined within charged pores, an increased distribution of counter ions has been proposed to be the cause. Under these circumstances, the amount of counter ions in the shells is enough to create the osmotic pressure needed, in order to achieve the measured resistances.

- Supplementing the dead-end experiments, a cross-flow setup was used, allowing direct visual observations of cake behavior to be made in real-time. This proved to be a very useful non-invasive tool for gaining a deeper understanding of filter cake structure and behavior. It was observed that higher surface charge results in a slower growing filter cake that also reaches a steady-state thickness more quickly. Furthermore, particles did not settle on first contact with the filter cake, but instead rolled along the cake surface until eventually settling in small depressions between other particles. The experiments confirmed the previously mentioned influence of particle charge on specific resistance and compressibility. It also showed compression and subsequent relaxation to be fast (within seconds) and reversible, while the degree of relaxation increased with particle charge. This underlines the notion of an increased osmotic pressure in the filter cake, due to the presence of counter ions associated with the charged surface.

Nomenclature

Roman letters

A	Membrane area (m^2)
b	Empirical parameters related to cake compressibility
CA	Concentration of carboxylic acid groups on particles (mol g_{DM}^{-1})
C_{avail}	Concentration of available counter ions, if evenly distributed in the pores (mol L^{-1})
C_π	Concentration of counter ions needed to obtain a certain osmotic pressure (mol L^{-1})
D_c	Particle diameter with collapsed shell (m)
d_i	The particle diameter below which i % of the particles are found
d_p	Pore diameter (nm)
D_s	Particle diameter with swollen shell (m)
EPS	Extracellular polymeric substances
h_{cake}	Filter cake height (μm)
HCP	Hexagonal close packed
HPC	Hydroxypropyl cellulose
J	Permeate flux (LMH, m s^{-1})
K	Empirical parameters related to cake compressibility
k	Kozeny constant
l	interparticle distance (nm)
n	Empirical parameters related to cake compressibility
Pa	Empirical parameters related to cake compressibility

PAA	Polyacrylic acid
P_{app}	Applied pressure (bar, Pa)
P_{eff}/P_{liq}	Effective/liquid pressure – equal to ΔP and TMP (bar, Pa)
Q_f	filtrate/permeate flow rate ($m^3\ s^{-1}$)
R	Hydraulic resistance (m^{-1})
R	particle radius (nm, μm)
R_f	Hydraulic resistance of fouling layer (m^{-1})
R_m	Membrane resistance (m^{-1})
s	Amount of dry matter deposited in the filter cake per volume of filtrate ($kg\ m^{-3}$)
S_0	volume specific surface area (m^{-1})
t	Filtration time (s)
t	time (s)
TMP	Pressure drop across the filter cake/membrane (bar, Pa)
U(t)	Degree of consolidation (t = 0 at transition point)
V(t)	Filtrate volume expelled at time t (m^3)
V_∞	Filtrate volume expelled at end of consolidation (m^3)
v_c	cake growth rate (μm ml^{-1})
Vc	Volume of wet filter cake
V_f	Filtrate/permeate volume (m^3)
V_{tr}	Filtrate volume expelled at transition point (m^3)

Greek letters

$\hat{\alpha}$	Average mass specific hydraulic resistance (m kg^{-1})
α	Mass specific hydraulic resistance (m kg^{-1})
α_0	The apparent zero-pressure specific resistance (m kg^{-1})
$\alpha_{K\text{-}C}$	Mass specific hydraulic resistance, calculated from the Kozeny-Carman equation (m kg^{-1})
$\hat{\alpha}_{max}$	Maximum specific resistance based on model from eq. 7 (m kg^{-1})
β	Empirical parameters related to cake compressibility
δ	Grade of polydispersity
ΔP	Pressure drop across the filter cake/membrane (bar, Pa)
$\Delta\pi$	Osmotic pressure in filter cake (bar, Pa)
ε	Porosity
ε_0	Apparent zero-pressure porosity
μ	Liquid viscosity (Pa s^{-1})
ρ	Density (kg m^{-3})
Φ	Solidosity
Φ_0	Apparent zero-pressure solidosity
Φ_{col}	solid volume fraction of a single particle = 1-ψ
Φ_{pack}	packing fraction of the swollen particles in the filter cake
Ψ	ratio between the volume of the fully swollen shell and the total particle volume

References

[1]   P. Larsen, Impact of Different Bacterial Species on Floc
        Characteristics in Activated Sludge, Section of Environmental
        Engineering, Aalborg Univeristy, Aalborg, 2007.

[2]   E. Ardern, W.T. Lockett, Experiments on the oxidation of sewage
        without the aid of filters, J. Soc. Chem. Ind. 33 (1914) 523–539.
        doi:10.1002/jctb.5000331005.

[3]   S.R. Austin, J.R. Livingston, L. Tortorici, Waste Activated Sludge
        Processing, 1980.

[4]   M.L. Christensen, The Effect of Filter Cake Viscoelasticity on
        Filtration - A Study of Activated Sludge Dewatering, Section of
        Chemistry, Aalborg University, Aalborg, 2006.

[5]   D.G. Parker, C.W. Randall, P.H. King, G. Parker, H. King,
        Biological conditioning for improved sludge filterability, Water
        Pollut. Control Fed. 44 (1972) 2066–2077.

[6]   F. Meng, S.-R. Chae, H.-S. Shin, F. Yang, Z. Zhou, Recent Advances
        in Membrane Bioreactors: Configuration Development, Pollutant
        Elimination, and Sludge Reduction, Environ. Eng. Sci. 29 (2011)
        139–160. doi:10.1089/ees.2010.0420.

[7]   G. Belfort, R.H. Davis, A.L. Zydney, The behavior of suspensions
        and macromolecular solutions in crossflow microfiltration, J. Memb.
        Sci. 96 (1994) 1–58. doi:10.1016/0376-7388(94)00119-7.

[8]   Y. Ye, V. Chen, P. Le-Clech, Evolution of fouling deposition and
        removal on hollow fibre membrane during filtration with periodical
        backwash, Desalination. 283 (2011) 198–205.
        doi:10.1016/j.desal.2011.03.087.

[9]   W.R. Bowen, F. Jenner, Theoretical descriptions of membrane
        filtration of colloids and fine particles: An assessment and review,
        Adv. Colloid Interface Sci. 56 (1995) 141–200. doi:10.1016/0001-
        8686(94)00232-2.

[10]   E.S. Tarleton, R.J. Wakeman, Understanding flux decline in
        crossflow microfiltration. Part 1 - Effects of particle and pore size,

Chem. Eng. Res. Des. 71 (1993) 399–410.

[11]   S. Lorenzen, Y. Ye, V. Chen, M.L. Christensen, Direct observation of fouling phenomena during cross-flow filtration: Influence of particle surface charge, J. Memb. Sci. 510 (2015) 546–558. doi:10.1016/j.memsci.2016.01.046.

[12]   A.L. Lim, R. Bai, Membrane fouling and cleaning in microfiltration of activated sludge wastewater, J. Memb. Sci. 216 (2003) 279–290. doi:10.1016/S0376-7388(03)00083-8.

[13]   W. Gao, H. Liang, J. Ma, M. Han, Z. Chen, Z. Han, et al., Membrane fouling control in ultrafiltration technology for drinking water production: A review, Desalination. 272 (2011) 1–8. doi:10.1016/j.desal.2011.01.051.

[14]   K. Kimura, T. Maeda, H. Yamamura, Y. Watanabe, Irreversible membrane fouling in microfiltration membranes filtering coagulated surface water, J. Memb. Sci. 320 (2008) 356–362. doi:10.1016/j.memsci.2008.04.018.

[15]   P.C. Carman, Review of literature, confirming validity of Kozeny's theory, Trans ICHemE. 15 (1937) 150–166.

[16]   G.E. Ogden, R.H. Davis, Experimental Determination of the Permeability and Relative Viscosity for Fine Latexes and Yeast Suspensions, Chem. Eng. Commun. 91 (1990) 11–28. doi:10.1080/00986449008940698.

[17]   G. Foley, A review of factors affecting filter cake properties in dead-end microfiltration of microbial suspensions, J. Memb. Sci. 274 (2006) 38–46. doi:10.1016/j.memsci.2005.12.008.

[18]   L.H. Mikkelsen, K. Keiding, Physico-chemical characteristics of full scale sewage sludges with implications to dewatering, Water Res. 36 (2002) 2451–2462. doi:10.1016/S0043-1354(01)00477-8.

[19]   P. Hodgson, G. Leslie, A. Fane, Cake resistance and solute rejection in bacterial microfiltration: the role of the extracellular matrix, J. Memb. Sci. 79 (1993) 35–53. doi:10.1016/0376-7388(93)85016-P.

[20]   D. Buckley, M. Madigan, J. Martinko, Brock Biology of Microorganisms, Pearson/Benjamin Cummings, 2013. doi:10.1017/CBO9781107415324.004.

[21]   L.H. Mikkelsen, T. Mascarenhas, P.H. Nielsen, Key parameters in sludge dewatering : testing for the shear sensitivity and EPS content, (2001) 105–114.

[22]   T. V Bugge, M.K. Jørgensen, M.L. Christensen, K. Keiding, Modeling cake buildup under TMP-step filtration in a membrane bioreactor: cake compressibility is significant., Water Res. 46 (2012) 4330–4338. doi:10.1016/j.watres.2012.06.015.

[23]   H.P. Chu, X.Y. Li, Membrane fouling in a membrane bioreactor (MBR): Sludge cake formation and fouling characteristics, Biotechnol. Bioeng. 90 (2005) 323–331. doi:10.1002/bit.20409.

[24]   R.M. Wu, D.J. Lee, C.H. Wang, J.P. Chen, R.B.H. Tan, Novel cake characteristics of waste-activated sludge, Water Res. 35 (2001) 1358–1362. doi:10.1016/S0043-1354(00)00513-3.

[25]   S.L.L. Birgitte L. Sørensen Kristian Keiding, A Theoretical Model for Blinding in Cake Filtration, Water Environ. Res. 69 (1997) 168–173. http://www.jstor.org/stable/25044859.

[26]   J.T. Novak, G.L. Goodman, A. Pariroo, J. Huang, The Blinding of Sludges During Filtration, Water Pollut. Control Fed. 60 (1988) 206–214.

[27]   F.M. Tiller, S. Haynes, W.-M. Lu, The role of porosity in filtration VII effect of side-wall friction in compression-permeability cells, AIChE J. 18 (1972) 13–20. doi:10.1002/aic.690180104.

[28]   F.M. Tiller, J.H. Kwon, Role of porosity in filtration: XIII. Behavior of highly compactible cakes, AIChE J. 44 (1998) 2159–2167. doi:10.1002/aic.690441005.

[29]   F.M. Tiller, C.S. Yeh, The role of porosity in filtration. Part XI: Filtration followed by expression, AIChE J. 33 (1987) 1241–1256. doi:10.1002/aic.690330803.

[30]   S. Lorenzen, M. Hinge, M.L. Christensen, K. Keiding, Filtration of core–shell colloids in studying the dewatering properties of water-swollen materials, Chem. Eng. Sci. 116 (2014) 558–566. doi:10.1016/j.ces.2014.05.029.

[31]   W.M. Lu, K.L. Tung, S.M. Hung, J.S. Shiau, K.J. Hwang, Compression of deformable gel particles, Powder Technol. 116

(2001) 1–12. doi:10.1016/S0032-5910(00)00357-0.

[32] P. Le-Clech, V. Chen, T.A.G. Fane, Fouling in membrane bioreactors used in wastewater treatment, J. Memb. Sci. 284 (2006) 17–53. doi:10.1016/j.memsci.2006.08.019.

[33] K. Ohmori, C.E. Glatz, Effects of pH and ionic strength on microfiltration of C. glutamicum, J. Memb. Sci. 153 (1999) 23–32. doi:10.1016/S0376-7388(98)00239-7.

[34] K. Ohmori, E. Iritani, Effect of addition of amino acids on microfiltration behavior of a microorganism slurry, J. Chem. Technol. Biotechnol. 79 (2004) 1169–1173. doi:10.1002/jctb.1047.

[35] K. Ohmori, C.E. Glatz, Effect of carbon source on microfiltration of Corynebacterium glutamicum, J. Memb. Sci. 171 (2000) 263–271. doi:10.1016/S0376-7388(00)00313-6.

[36] T. V. Bugge, P. Larsen, A.M. Saunders, C. Kragelund, L. Wybrandt, K. Keiding, et al., Filtration properties of activated sludge in municipal MBR wastewater treatment plants are related to microbial community structure, Water Res. 47 (2013) 6719–6730. doi:10.1016/j.watres.2013.09.009.

[37] K. Keiding, M.R. Rasmussen, Osmotic effects in sludge dewatering, Adv. Environ. Res. 7 (2003) 641–645. doi:10.1016/S1093-0191(02)00043-6.

[38] J.G. Wijmans, S. Nakao, C.A. Smolders, Flux limitation in ultrafiltration: Osmotic pressure model and gel layer model, J. Memb. Sci. 20 (1984) 115–124. doi:10.1016/S0376-7388(00)81327-7.

[39] J. Chen, M. Zhang, A. Wang, H. Lin, H. Hong, X. Lu, Osmotic pressure effect on membrane fouling in a submerged anaerobic membrane bioreactor and its experimental verification., Bioresour. Technol. 125 (2012) 97–101. doi:10.1016/j.biortech.2012.08.038.

[40] Y. Zhang, M. Zhang, F. Wang, H. Hong, A. Wang, J. Wang, et al., Membrane fouling in a submerged membrane bioreactor: effect of pH and its implications., Bioresour. Technol. 152 (2014) 7–14. doi:10.1016/j.biortech.2013.10.096.

[41] M. Zhang, W. Peng, J. Chen, Y. He, L. Ding, A. Wang, et al., A new insight into membrane fouling mechanism in submerged membrane

bioreactor: osmotic pressure during cake layer filtration., Water Res. 47 (2013) 2777–86. doi:10.1016/j.watres.2013.02.041.

[42]   D. Curvers, S.P. Usher, A.R. Kilcullen, P.J. Scales, H. Saveyn, P. Van der Meeren, The influence of ionic strength and osmotic pressure on the dewatering behaviour of sewage sludge, Chem. Eng. Sci. 64 (2009) 2448–2454. doi:10.1016/j.ces.2009.01.043.

[43]   R.H. Davis, Modeling of Fouling of Crossflow Microfiltration Membranes, Sep. Purif. Rev. 21 (1992) 75–126. doi:10.1080/03602549208021420.

[44]   H. Li, A.G. Fane, H.G.L. Coster, S. Vigneswaran, Direct observation of particle deposition on the membrane surface during crossflow micro Filtration, J. Memb. Sci. 149 (1998) 83–97.

[45]   P. Le-Clech, Y. Marselina, Y. Ye, R.M. Stuetz, V. Chen, Visualisation of polysaccharide fouling on microporous membrane using different characterisation techniques, J. Memb. Sci. 290 (2007) 36–45. doi:10.1016/j.memsci.2006.12.012.

[46]   K.-J. Hwang, C.-L. Hsueh, Dynamic analysis of cake properties in microfiltration of soft colloids, J. Memb. Sci. 214 (2003) 259–273. doi:10.1016/S0376-7388(02)00556-2.

[47]   M.L. Christensen, P. Sedin, H. Theliander, K. Keiding, Pressure and concentration profiles in filter cake consisting of core/shell latex particle, Colloids Surfaces A Physicochem. Eng. Asp. 290 (2006) 295–303. doi:10.1016/j.colsurfa.2006.05.037.

[48]   J. Altmann, S. Ripperger, Particle deposition and layer formation at the crossflow microfiltration, J. Memb. Sci. 124 (1997) 119–128. doi:10.1016/S0376-7388(96)00235-9.

[49]   R. Faibish, M. Elimelech, Y. Cohen, Effect of Interparticle Electrostatic Double Layer Interactions on Permeate Flux Decline in Crossflow Membrane Filtration of Colloidal Suspensions: An Experimental Investigation., J. Colloid Interface Sci. 204 (1998) 77–86. doi:10.1006/jcis.1998.5563.

[50]   C. Shen, W.B. Russel, F.M. Auzerais, Colloidal gel filtration: Experiment and theory, AIChE J. 40 (1994) 1876–1891. doi:10.1002/aic.690401111.

[51] M.L. Christensen, C. Johansson, M. Sedin, K. Keiding, Nonlinear filtration behavior of soft particles: Effect of dynamic cake compression, Powder Technol. 207 (2011) 428–436. doi:10.1016/j.powtec.2010.11.031.

[52] M.L. Christensen, T.B. Nielsen, M.B.O. Andersen, K. Keiding, Effect of water-swollen organic materials on crossflow filtration performance, J. Memb. Sci. 333 (2009) 94–99. doi:10.1016/j.memsci.2009.02.007.

[53] A.K. Van Helden, J.W. Jansen, A. Vrij, Preparation and characterization of spherical monodisperse silica dispersions in nonaqueous solvents, J. Colloid Interface Sci. 81 (1981) 354–368. doi:10.1016/0021-9797(81)90417-3.

[54] V.M. Gun'ko, V.I. Zarko, R. Leboda, E. Chibowski, Aqueous suspension of fumed oxides: Particle size distribution and zeta potential, Adv. Colloid Interface Sci. 91 (2001) 1–112. doi:10.1016/S0001-8686(99)00026-3.

[55] H. Kawaguchi, Functional polymer microspheres, Prog. Polym. Sci. 25 (2000) 1171–1210. doi:10.1016/S0079-6700(00)00024-1.

[56] P. Borget, F. Lafuma, C. Bonnet-Gonnet, Characterizations and properties of hairy latex particles, J. Colloid Interface Sci. 285 (2005) 136–145. doi:10.1016/j.jcis.2004.11.019.

[57] R. Arshady, Suspension, emulsion, and dispersion polymerization: A methodological survey, Colloid Polym. Sci. 270 (1992) 717–732. doi:10.1007/BF00776142.

[58] E.S. Daniels, E.D. Sudol, M.S. El-Aasser, Polymer colloids: science and technology of latex systems, American Chemical Society, 2002.

[59] S. Lorenzen, M.L. Christensen, Organic model particles with controllable size and surface charge; synthesis, characterization and microfiltration analysis, Powder Technol. (submitted October 2016 - under review).

[60] S. Kawaguchi, K. Ito, Dispersion polymerization, Adv. Polym. Sci. 175 (2005) 299–328. doi:10.1007/b100118.

[61] K.E.J. Barret, ed., Dispersion Polymerization in Organic Media, Wiley, 1974.

[62]   A.J. Paine, Y. Deslandes, P. Gerroir, B. Henrissat, Dispersion polymerization of styrene in polar solvents: I. Grafting Mechanism of Stabilization by Hydroxypropyl Cellulose, J. Colloid Interface Sci. 138 (1990) 170–181. doi:10.1016/0021-9797(90)90192-Q.

[63]   Y.M. Wang, C.Y. Pan, Study of the mechanism of the emulsifier-free emulsion polymerization of the styrene/4-vinylpyridine system, Colloid Polym. Sci. 277 (1999) 658–665. doi:10.1007/s003960050437.

[64]   A.J. Paine, W. Luymes, J. McNulty, Dispersion polymerization of styrene in polar solvents. 6. Influence of reaction parameters on particle size and molecular weight in poly(N-vinylpyrrolidone)-stabilized reactions, Macromolecules. 23 (1990) 3104–3109. doi:10.1021/ma00214a012.

[65]   V. Bulmuş, A. Tuncel, E. Pişkin, Production of polymethylmethacrylate particles by dispersion polymerization in aqueous media with ceric ammonium nitrate, J. Appl. Polym. Sci. 60 (1996) 697–704. doi:10.1002/(SICI)1097-4628(19960502)60:5<697::AID-APP6>3.0.CO;2-L.

[66]   S. Shen, E. Sudol, M. El-Aasser, Control of particle size in dispersion polymerization of methyl methacrylate, J. Polym. Sci. Part A Polym. Chem. 31 (1993) 1393–1402. doi:10.1002/pola.1993.080310606.

[67]   M.P. Stevens, Polymer Chemistry: An Introduction, Oxford University Press, 1999.

[68]   S. Shen, E.D. Sudol, M.S. El-Aasser, Dispersion polymerization of methyl methacrylate: Mechanism of particle formation, J. Polym. Sci. Part A Polym. Chem. 32 (1994) 1087–1100. doi:10.1002/pola.1994.080320611.

[69]   Y. Chen, W. Norde, H.C. Van Der Mei, H.J. Busscher, Bacterial Cell Surface Deformation under External Loading, MBio. 3 (2012) 1–7. doi:10.1128/mBio.00378-12.Editor.

[70]   P.H. Wang, C.-Y. Pan, Emulsion copolymerization of styrene with acrylic or methacrylic acids - distribution of the carboxylic group, Colloid Polym. Sci. 279 (2001) 98–103. doi:10.1007/s003960000407.

[71]   C. Tropea, A.L. Yarin, J.F. Foss, Springer handbook of experimental

fluid mechanics, Springer, 2007. doi:10.1007/978-3-540-30299-5.

[72]   H. Ohshima, Electrophoretic mobility of soft particles, Colloids
         Surfaces A Physicochem. Eng. Asp. 103 (1995) 249–255.
         doi:10.1016/0927-7757(95)03293-M.

[73]   S. Lorenzen, K. Keiding, M.L. Christensen, The effect of particle
         surface charge density on filter cake properties during dead-end
         filtration, Chem. Eng. Sci. (submitted October 2016 - under review).

[74]   N.P.R. Andersen, M.L. Agerbæk, K. Keiding, Measurement of
         electrokinetics in cake filtration, Colloids Surfaces A Physicochem.
         Eng. Asp. 213 (2003) 27–36. doi:10.1016/S0927-7757(02)00333-3.

[75]   M. Shirato, T. Murase, M. Iwata, S. Nakatsuka, The Terzaghi-Voigt
         combined model for constant-pressure consolidation of filter cakes
         and homogeneous semi-solid materials, Chem. Eng. Sci. 41 (1986)
         3213–3218. doi:http://dx.doi.org/10.1016/0009-2509(86)85059-X.

[76]   R.J. Wakeman, E.S. Tarleton, Filtration: Equipment Selection,
         Modelling and Process Simulation, Elsevier Advanced Technology,
         1999.

[77]   S.G. Sveegaard, K. Keiding, M.L. Christensen, Compression and
         swelling of activated sludge cakes during dewatering., Water Res. 46
         (2012) 4999–5008. doi:10.1016/j.watres.2012.06.039.

[78]   E.M. Johnson, W.M. Deen, Hydraulic permeability of agarose gels,
         AIChE J. 42 (1996) 1220–1224. doi:10.1002/aic.690420504.

[79]   M.L. Christensen, N.P.R. Andersen, M. Hinge, K. Keiding,
         Characterisation of the transition between the filtration and
         consolidation stage from liquid pressur measurements, Filtration. 6
         (2006) 71–78.

[80]   L.C. Graton, H.J. Fraser, Systematic Packing of Spheres: With
         Particular Relation to Porosity and Permeability, J. Geol. 43 (1935)
         785–909. http://www.jstor.org/stable/30058420.

[81]   D.G. Grier, Colloids: a surprisingly attractive couple, Nature. 393
         (1998) 621–623. doi:Doi 10.1038/31340.

[82]   E.A. Larsen, G.D. Grier, Electrodynamical Like-Charge Attractions
         in Metastable Colloidal Crystallites, Nature. 385 (1997) 230–233.

doi:10.1142/S0217984998001013.

[83]   W.R. Bowen, A.O. Sharif, Long-range electrostatic attraction between like-charge spheres in a charged pore, Nature. 393 (1998) 663–665. doi:10.1038/31418.

[84]   A. Sofia, W.J. Ng, S.L. Ong, Engineering design approaches for minimum fouling in submerged MBR, Desalination. 160 (2004) 67–74. doi:10.1016/S0011-9164(04)90018-5.

[85]   M.M. Rahman, M.H. Al-Malack, Performance of a crossflow membrane bioreactor (CF-MBR) when treating refinery wastewater, Desalination. 191 (2006) 16–26. doi:10.1016/j.desal.2005.05.022.

[86]   T. Stephenson, K. Brindle, S. Judd, B. Jefferson, Membrane Bioreactors for Wastewater Treatment, IWA Publishing, 2000. https://books.google.dk/books?id=XZ3bCwAAQBAJ.